Mesoscale Snowfall Prediction and Verification in Mountainous Terrain

MELANIE WETZEL,* MICHAEL MEYERS,+ RANDOLPH BORYS,* RAY MCANELLY,# WILLIAM COTTON,# ANDREW ROSSI,* PAUL FRISBIE,+ DAVID NADLER,+ DOUGLAS LOWENTHAL,* STEPHEN COHN,@ AND WILLIAM BROWN@

*Desert Research Institute, Reno, Nevada
+National Weather Service, Grand Junction, Colorado
#Colorado State University, Fort Collins, Colorado
@National Center for Atmospheric Research, Boulder, Colorado

(Manuscript received 12 June 2003, in final form 29 March 2004)

ABSTRACT

Short-term forecasting of precipitation often relies on meteorological radar coverage to provide information on the intensity, extent, and motion of approaching mesoscale features. However, in significant portions of mountainous regions, radar coverage is lacking because of topographic blocking, and the absence of radar signatures in sections of the radar scan produces uncertain or even misleading information to the public and operational forecasters. In addition, echo characteristics within the radar volume scan are often influenced by the vertical extent and type of precipitation. Each of these conditions limits the opportunity for accurate snowfall prediction and studies of precipitation climatology. To improve both short-term forecasting and postevent verification studies, much greater use can be made of specifically sited surface observations, tailored graphical output from mesoscale models, satellite remote sensing, and case study knowledge of local topographic influences. In this paper, methods to support snowfall forecasts and verification in radar-limited mountainous terrain are demonstrated that include matching the output parameters and graphics from high-resolution mesoscale models to surface mesonets and snowfall observations, analysis of continuous and event-based measurements of snow density, application of multispectral satellite data for verification and trend analysis, and characterization of orographic influences in different winter storm scenarios. The advantages of improved wintertime quantitative precipitation forecasting (QPF) in mountain regions include public safety responsibilities that are critical to National Weather Service (NWS) operations, and are relevant to any mountainous region with radar scan limitations or during periods of radar data outages.

1. Introduction

Many regions of the Intermountain West have restricted radar coverage, due to the complex terrain, that causes uncertainty and bias in precipitation analysis and short-term (0–12 h) forecasting. Approximately 20 of the Weather Surveillance Radar-1988 Doppler (WSR-88D) are atop mountain terrain. Because of scanning strategies designed for flatland radars, radar signals at the lowest elevation angle do not adequately detect low-altitude weather events (Wood et al. 2003). Radar coverage is very limited at heights of 1, 2, and 3 km above ground level, which limits the usefulness of the radar data and quantitative precipitation estimation (Maddox et al. 2002). Beam blockage in complex topography regions may also impact full detection of the precipitation signature. In addition, the lack of observed precipitation patterns leads to gaps in knowledge of mesoscale precipitation climatology that might otherwise aid QPF analysis for time scales longer than 12 h. Technique development for quantitative snowfall forecasts in orographic terrain is needed, particularly when radar data coverage is degraded by topography. As with satellite imagery, time-lapse animations of radar imagery are used whenever possible to anticipate and verify the evolution of storm events. Operational forecasters with local knowledge of radar scan limitations can often recognize how precipitation echo patterns change due to the effects of topography on detectable scan volume. This is particularly true in winter when snowfall is generated from more stratiform cloud systems rather than deep convection.

The public has wide access to radar scan graphics, but without an experienced eye someone may assume that no precipitation exists and disregard short-term precipitation forecasts that impact their decision-making for road or private air travel. Improved interpretation can be provided to the public by National Weather Service (NWS) statements and broadcast weather information, focusing on both the reason for limited radar

Corresponding author address: Melanie A. Wetzel, Division of Atmospheric Sciences, Desert Research Institute, 2215 Raggio Parkway, Reno, NV 89512-1095.
E-mail: wetzel@dri.edu

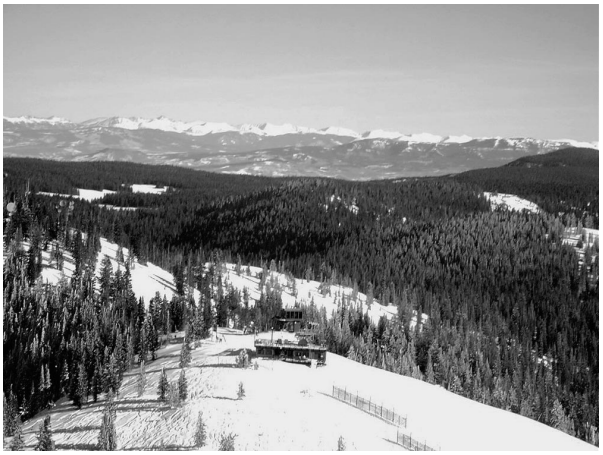

FIG. 1. DRI Storm Peak Laboratory at 3200-m elevation along the ridge of the Park Range of northern Colorado.

FIG. 2. NCAR Multiple Antenna Profiling Radar (foreground) and Park Range (background).

coverage and the use of other sources to fill the gap for short-term forecasting of precipitation. In geographic areas with limited radar coverage, these other sources of information become critical to forecast verification and trend analysis, for the operational forecast office as well as the general public. Quantitative forecasting of snowfall, in terms of physical depth accumulations, is also limited by uncertainty in the density of the falling snow. Many forecast applications (such as highway maintenance, traffic warnings, avalanche control, and ski area operations) are more sensitive to accurate prediction of physical snow-depth accumulation than snow water equivalent (SWE). Previous studies of fallen-snow density indicate the wide variety of snow densities encountered (Judson and Doesken 2000) and the role of many factors related to in-cloud microphysics and subcloud transformation (Roebber et al. 2003).

In general, mountainous regions provide enhanced precipitation rates and accumulations due to orographic uplift. The rate of snowfall accumulation during winter precipitation events is directly related to the efficiency of snow growth processes, and these processes include both kinematic forcing associated with orographic uplift as well as the microphysical structure conducive to rapid crystal growth and settling. Heggli and Rauber (1988) have shown that much of the supercooled liquid water that contributes to heavy snowfall is typically located in the lowest kilometer above the terrain, and Reinking et al. (2000) describe the important process by which ice crystals generated from higher elevations in ''seeder'' cloud regions grow rapidly by accretion in the ''feeder'' cloud below. The near-infrared image channel on the Geostationary Operational Environmental Satellite (GOES) is useful in monitoring cloud structure forced by these orographic effects. Satellite observations of the cloud-top region can reveal particle size and phase characteristics. If the cloud-top region contains supercooled droplets, the near-infrared signature shown in the satellite image data can aid in identifying the glaciation process (Wetzel 1995), which indicates the availability of ice crystals for efficient snow growth. By combining satellite remote sensing information on the structure and evolution of the cloud system with kinematic and thermodynamic data from observations and mesoscale model output, the forecasting process can incorporate analysis techniques specific to orographic scenarios.

This paper presents techniques that can be used to improve the accuracy of quantitative snowfall forecasting and analysis in mountainous regions. Data from a research program on winter orographic precipitation processes provide the framework within which to demonstrate the value of adding auxiliary resources such as targeted sensor systems at high-altitude sites, satellite remote sensing methods, creation of a local snowfall climatology, and mesoscale modeling with graphical products tailored to orographic forecasting. The added benefit of this approach is examined in case studies for a specific mountain range in the northern Colorado Rocky Mountains.

2. Field study overview

This research uses case studies of well-documented snowfall events over a north–south-oriented mountain ridge to evaluate the effects on snowfall production due to mesoscale dynamics, mixed-phase cloud microphysics, and thermodynamic profiles over orographic terrain, and to apply procedures designed to improve short-term forecasting of snowfall in this environment. The study was based at the Desert Research Institute's Storm Peak Laboratory (SPL) (Fig. 1), located in the Park Range near Steamboat Springs in northwest Colorado. This high-elevation (3220 m MSL; typically ~700 hPa pressure level) research lab has been used for over 20 years to conduct basic research on cloud physics, cloud–aerosol interactions, and alpine radiation climatology (Borys and Wetzel 1997; Borys et al. 2000; Lowenthal et al. 2002).

The study was conducted in tandem with ongoing research related to the microphysical processes that de-

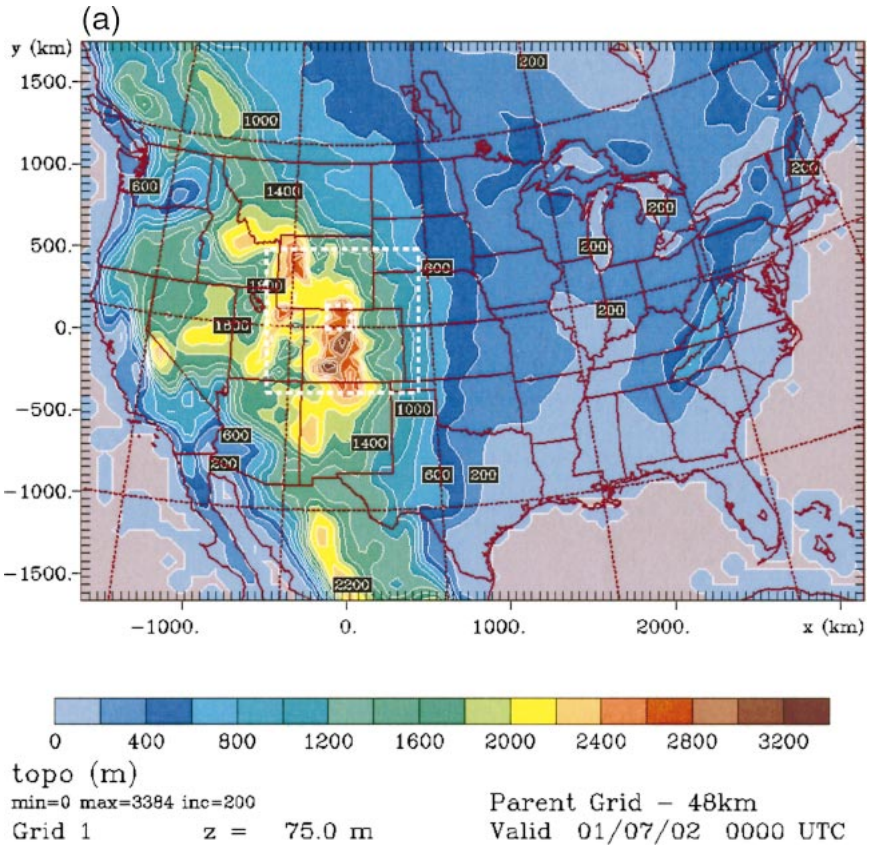

FIG. 3. (a) Nested-grid configuration for the RAMS model. The parent (outer) grid over the conterminous U.S. has a 48-km horizontal resolution. The regional grid (12-km resolution) is centered over Colorado, and the inner fine-mesh grid (3-km resolution) is centered on the Park Range of northern Colorado. Color shading indicates topographic elevation. Distances shown on the edge of the figure are relative to the center of the model's grid 2 (12 km) regional domain. (b) RAMS model fine-mesh (3-km grid resolution) domain and color contours showing topographic elevation within that domain, with site identifiers including Steamboat Springs (SBS), Yampa Valley, Park Range (in central portion of figure), the Flat Tops Mountains (southwest corner), and Never Summer Range (eastern edge of domain). The Park Range is well defined by the 2800-m contour line. Distances shown on the edge of the figure are relative to the center of the model's grid 2 (12 km) regional domain. (c) Detail of terrain in the study region shown by shaded contours of topographic elevation. Snow sampling sites are indicated by identifiers at VLW, RAD, VLV, CHP, and PHQ. Other locations indicated are the Storm Peak Laboratory (SPL) and Steamboat Springs (SBS), as well as the SNOTEL sites at Dry Lake (DRLK) and Tower (TOWR) in the vicinity. Distances shown on the edge of the figure are relative to the center of the model's grid 2 (12 km) regional domain.

termine snowfall production in orographic cloud systems. Research described here included the deployment of a high-resolution vertically profiling radar (Fig. 2) from the National Center for Atmospheric Research (NCAR), local rawinsonde soundings, meteorological mesonet data collection, ridge-top cloud and precipitation microphysical measurements, snow core sampling at multiple elevations, and numerical model simulations to evaluate snow accumulation forecasts for a 3-km-resolution mesoscale grid centered over the mountain range. Data collection was conducted January–March 2001 and 2002 as well as December 2002.

In the series of in situ microphysical measurements at SPL, cloud droplet size distributions were measured using an aspirated Droplet Measurement Technologies (DMT) SPP-100 forward scattering spectrometer probe. Ice crystal size distributions, ice water contents, and two-dimensional images were sampled using a Particle Measurement Systems 2DP optical array probe. These two microphysics instruments were mounted on a large vane that orients the sample inlet to the oncoming airflow. Computer control of the sample data provided 10-s instantaneous values plus 6-min averages and integrated sample statistics for number, area and volume size distributions, liquid water content, mean and modal droplet sizes, and other parameters. Ice crystal habit, dimensions, and masses were also obtained from the Desert Research Institute (DRI) Snow Video Spectrometer sys-

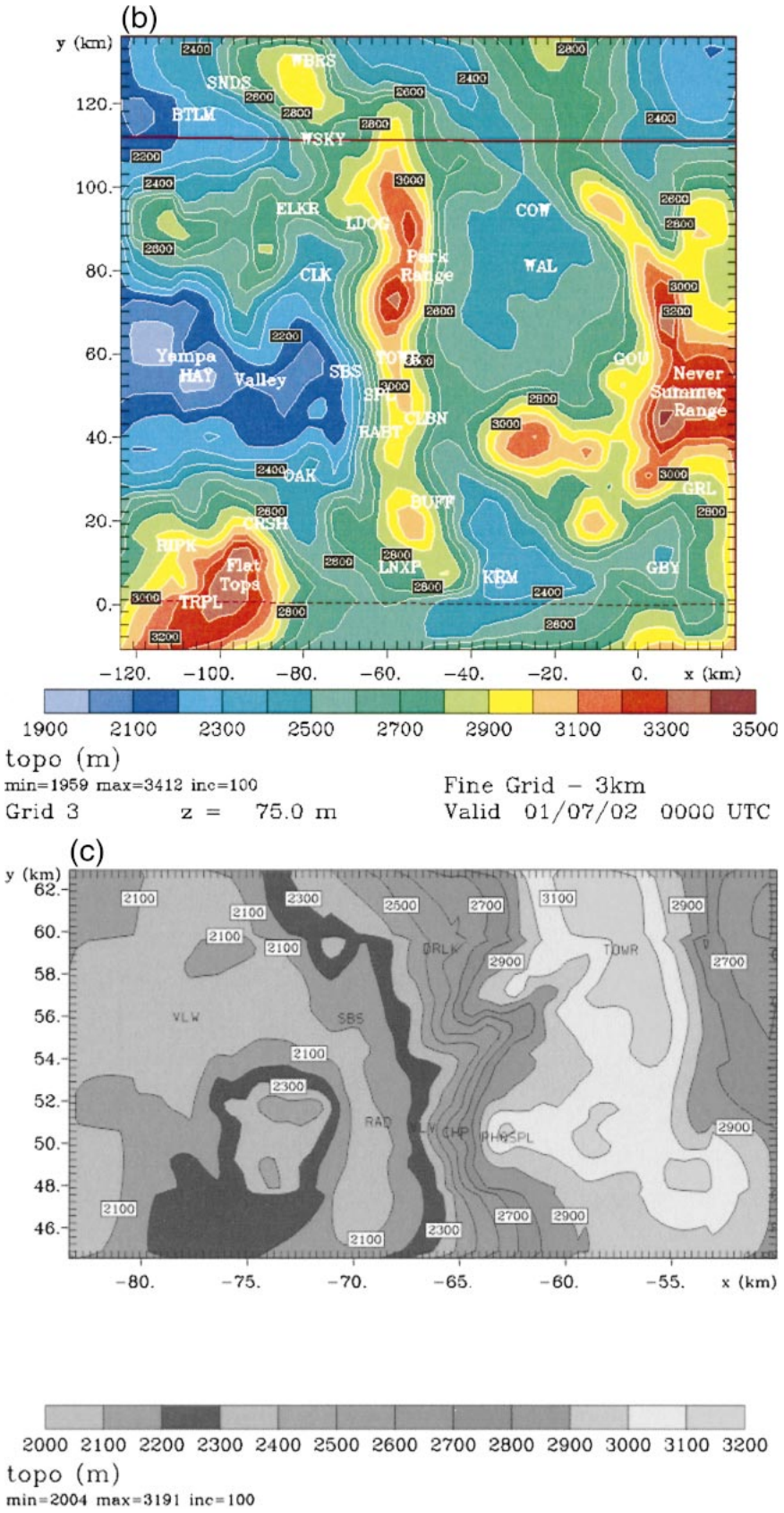

FIG. 3. (*Continued*)

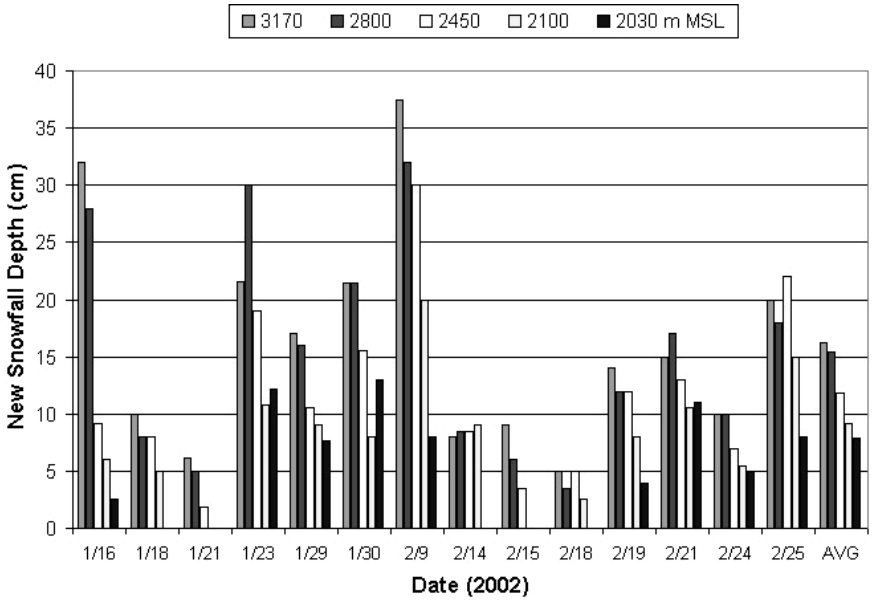

FIG. 4. Event time series of snow depth accumulation for sampling sites at elevations from 2030 to 3170 m MSL (6664–10 410 ft).

tem (Borys et al. 2000). Cloud sieves were used to sample the volume concentration and mass flux of supercooled liquid water in cloud, and flow-oriented bag samplers provided measurements of precipitation mass flux. A high-precision OHAUS mass gauge fitted with a large collection pan and located within a snow-collection wind shelter was used to measure time series of snowfall mass accumulation at 1-min intervals. A continuously recording meteorological tower system provided 5-min average and 10-s maximum values of variables such as wind speed and direction, air temperature, relative humidity, solar radiation, ozone, aerosol concentration, and additional atmospheric conditions. These data contributed to the analysis of cloud and precipitation events.

A transect of snowfall measurement sites was established along an east–west track, beginning west of Steamboat Springs on the Yampa Valley floor, approximately 10 km from the base of the mountain range, and continuing with four sites of increasing elevation from the NCAR radar (RAD) at the base of the mountain, at intervals of 400 m to the ski area Patrol Head-

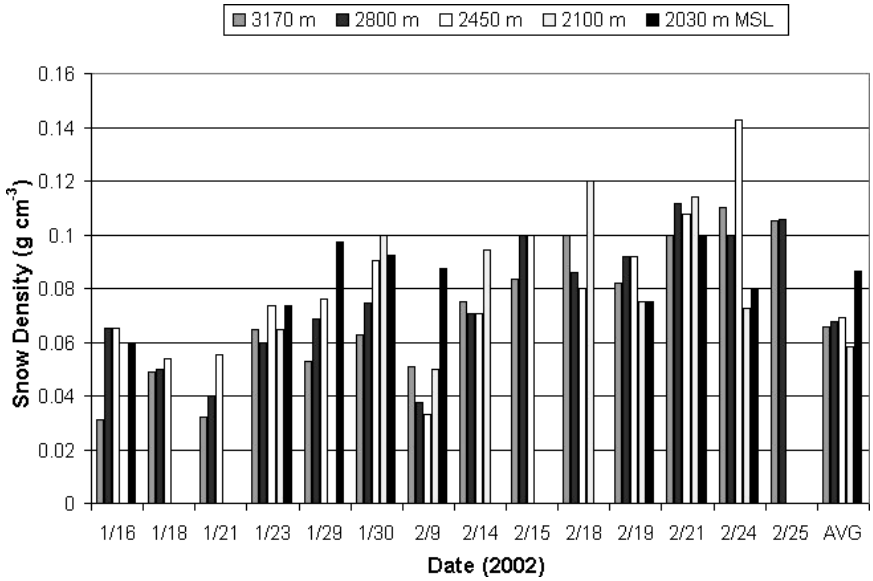

FIG. 5. As in Fig. 4 but for snow density.

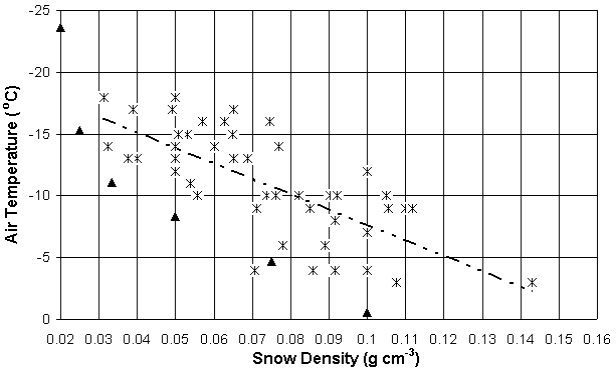

FIG. 6. Scatterplot showing the relationship between air temperature and new snow density (stars) obtained from three sampling locations (at 2450, 2800, and 3170 MSL) in the Park Range during winter months of 2002, with linear curve fit (dashed line). Also shown are breakpoints (triangles) obtained from the NWS meltwater conversion table.

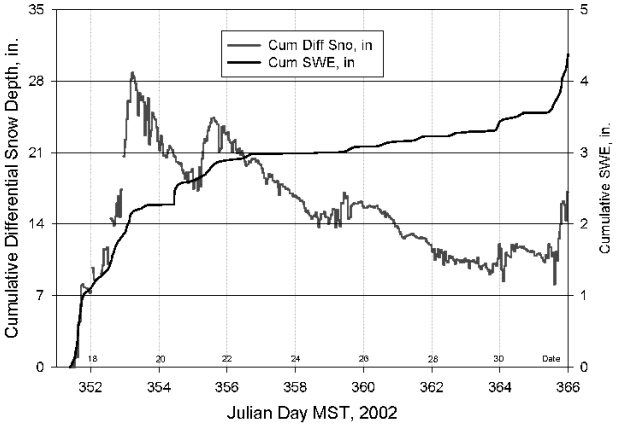

FIG. 7. Time series of differential snow depth obtained from an acoustic snow sensor and cumulative SWE depth measured by an antifreeze-type tipping-bucket gauge at the Patrol Headquarters site for the last 2 weeks of Dec 2002. The differential snow depth increases during snow events and then decreases between snow periods, primarily because of snow settling.

quarters (PHQ) along the mountain ridge (approximately centered within Fig. 2). Measurements were made of the following parameters in the core of new snow accumulated on snow boards: new snow depth (cm), average density (g cm^{-3}), total snow water equivalent (SWE, mm), temperature (°C), crystal type [classification based on Magono and Lee (1966)], crystal size (mm), degree of crystal riming, and profiles of new snow layer density (g cm^{-3}) in 2-cm depth layer intervals. The snow boards were not surrounded by a shielding device but were located in tree-shielded areas for sampling sites in the mountain locations. This tree sheltering method has been used to collect ''ground truth'' snow accumulation measurements for previous studies of gauge accuracy (Goodison 1978), and it is expected that surface-level winds at the snow boards did not often exceed threshold speeds associated with surface snow transport (Li and Pomeroy 1996).

New snow depth from each precipitation event was measured as a total accumulation on a snow board. The snow board used was a 60 cm by 60 cm square and was cleared after each measurement (which varied in time based on snowfall accumulation). Snow board core density was measured using a Snowmetrics T1 tube sampler and a hanging scale. New snow layer density was measured using a 66.6 cm^3 stainless cutter and an Acculab VI-4kg digital flat scale. Other observations included snow layer temperature, air temperature, wind, and snow occurrence at the sample time. The sites were selected with some surrounding vegetation where possible to reduce the effects of wind on snowpack modification but were located within sufficient clearing space to minimize undercapture. When possible, the data collection sites were located near established meteorological data collection sites. Snow sampling was conducted on a storm event basis during 16 January–25 February 2002. A majority of the measurements took place while the snow event was still occurring, which reduced the effects of snowpack metamorphosis, and the comparative analysis with model forecasts was carried out on the snowfall accumulation up to that point in time (rather than the ''total'' snowfall for a given event).

A mesonet of surface meteorological reporting stations is operated continuously by the Steamboat Ski and Resort Corporation (SSRC) on the western face of the mountain ridge to support their snowmaking activities. This mesonet provided hourly time series measurements of temperature and relative humidity. SSRC operates an acoustic sensor along the ridge at PHQ that was used to monitor physical snow depth, which was very useful in establishing the time sequence of snowfall accumulation. The acoustic sensor also provides a record of snow depth loss due to snowpack metamorphosis. DRI operates an antifreeze tipping-bucket precipitation gauge collocated with the acoustic snow sensor. This

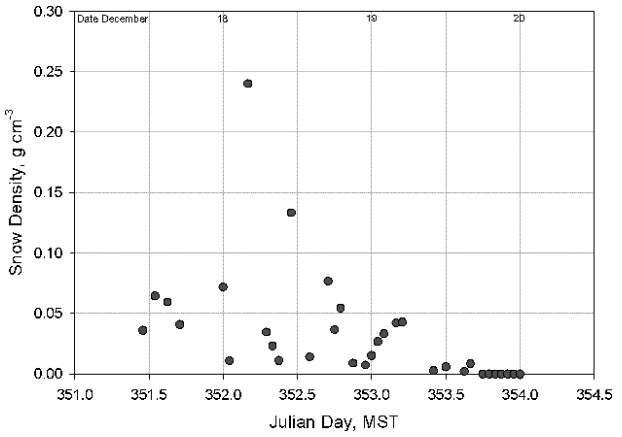

FIG. 8. Time series of new snow density estimated for the first 3 days of the dataset shown in Fig. 7.

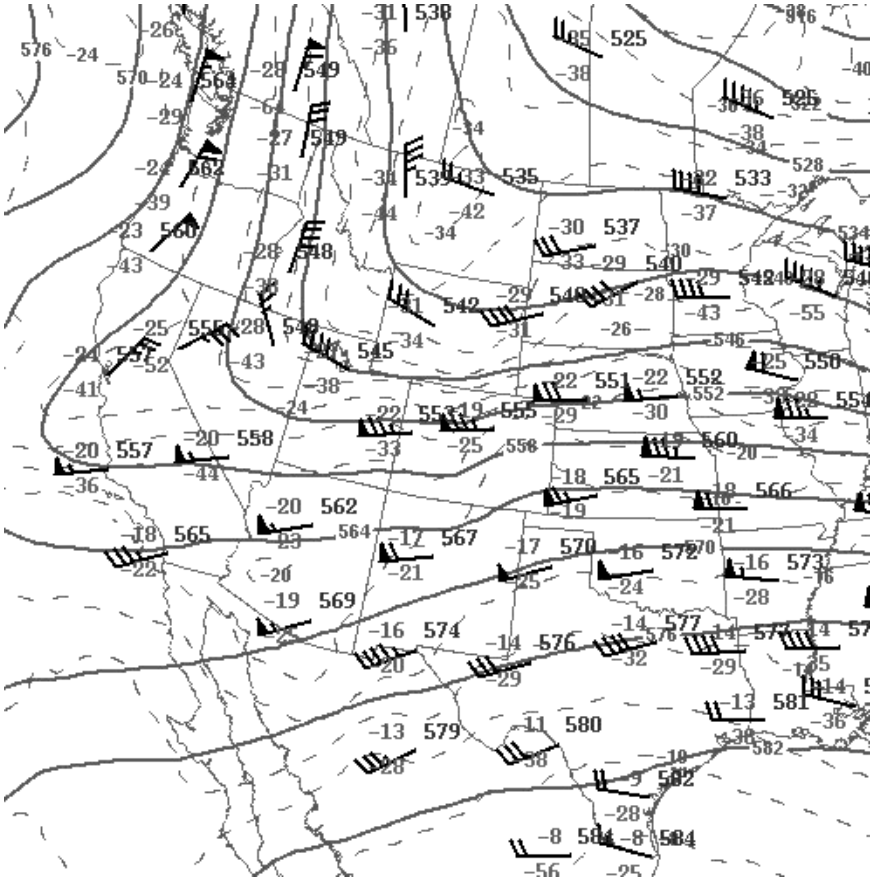

FIG. 9. The 500-hPa analysis of winds (barbs, kt), temperatures (dashed contours °C), dewpoints (no contours °C), and heights (solid contours, dam) for 0000 UTC 16 Jan 2002. This figure was obtained from the NOAA Storm Prediction Center (http://www.spc.noaa.gov).

was also the highest-elevation site of the snow measurement transect (PHQ).

The Multiple Antenna Profiler Radar (MAPR) is an advanced wind profiling radar developed by the NCAR Atmospheric Technology Division (ATD) to make rapid wind measurements in the lower troposphere. Instrument design is based on a 915-MHz wind-profiling radar that has been modified to use the spaced antenna wind measurement technique (Cohn et al. 2001). The system has one transmitter and four vertically pointing antenna subarrays for reception. The motion of the reflected signal across the array is tracked to calculate wind velocity. Output parameters include horizontal wind, Doppler (radial) velocity, volume reflectivity, and velocity variance. Time frequency is typically 60 s and vertical resolution modes are 50–200 m. The MAPR was operated at the RAD site, a valley elevation on the western edge of the Park Range, during mid-January to early March 2002. The ATD GPS-Loran Atmospheric Sounding System (GLASS) provided balloon profile data during event periods, and surface meteorological measurements (pressure, temperature, wind, humidity, radiation, and precipitation) were conducted at the radar continuously during the study period.

The Regional Atmospheric Modeling System (RAMS) model (Cotton et al. 2003) Version 4.29 developed at Colorado State University (CSU) was set up to run nominally twice daily (0000 and 1200 UTC cycles) in real time at CSU in support of the field campaigns at SPL. A nested-grid configuration similar to that described by Meyers et al. (2001) was used, in which parent, regional, and fine grids, respectively, covered the conterminous United States, Colorado, and portions of adjacent states, and a 150 km $\times$ 150 km domain centered on the Park Range, at 48-, 12- (Fig. 3a), and 3-km (Fig. 3b) grid spacing. A closer view of the study area with locations of sampling sites is shown in Fig. 3c. The terrain-following sigma-z vertical coordinate system was represented by 36 levels, with grid spacing stretching from $<$150 m near the surface to approximately 1000 m at and above 9 km.

The RAMS model used the single-moment, mixed-phased microphysical scheme described by Walko et al. (1995), with prognostic fields for cloud droplets, rain,

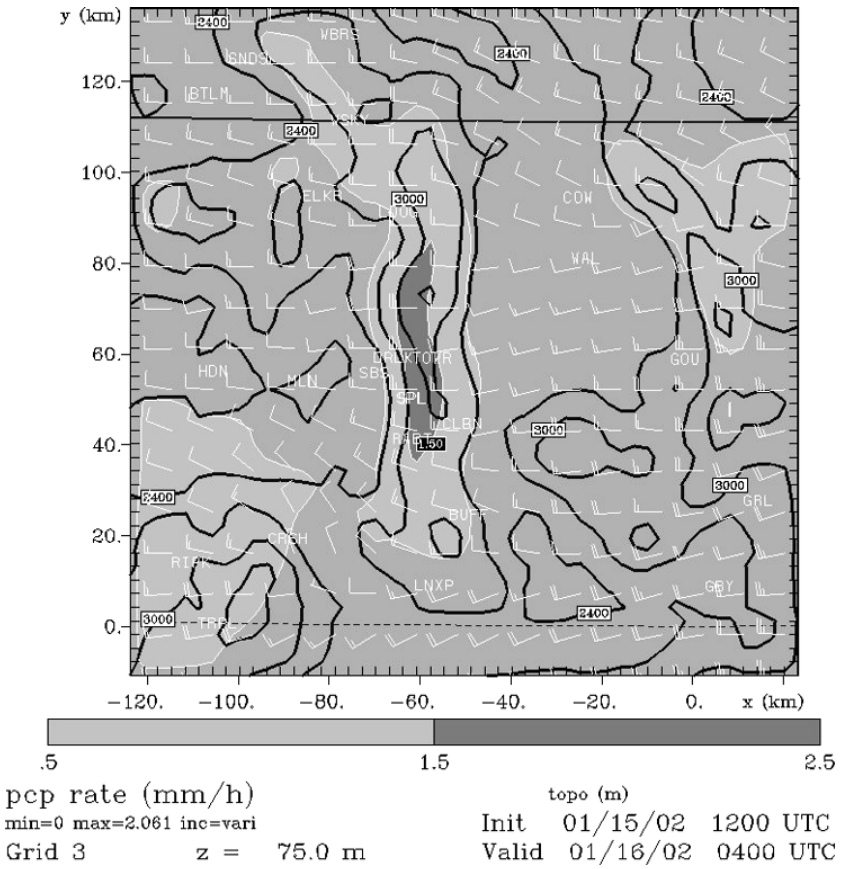

FIG. 10. RAMS model precipitation rate forecast at 0400 UTC 16 Jan 2002. Wind barbs (m s^{-1}) indicate horizontal wind velocities at the 75-m grid level, and black contours indicate model topography (elevation in m).

pristine ice crystals, snow, aggregates, graupel, and hail (Meyers et al. 1992; Meyers and Cotton 1992). Hydrometeor sizes were distributed according to a gamma function. For each forecast cycle, the RAMS initialization and time-dependent lateral and top boundary conditions were based on operational Eta model initial data and 6-hourly forecasts from the same cycle. These Eta datasets were obtained electronically as soon as they became available from the National Centers for Environmental Prediction. They were in gridded binary (GRIB) format on the Advanced Weather Interactive Processing System (AWIPS) grid 211 (Dey 1998), with about 80-km horizontal spacing and at 19 pressure levels at 50-hPa intervals. The RAMS simulations were run on a Linux-based PC cluster with usually about 20 processors working in parallel. The nonhydrostatic simulations were ''cold started'' about 3 h after the initial time and required about 5 h to complete the 48 h forecast period. Graphical forecast products were generated at 2-h intervals and made available to operational users on CSU's RAMS Web site. For the few forecast cycles that failed to run in real time or where the fine grid was located elsewhere in the regional grid, after-the-fact forecast simulations for cases of interest to this project were completed identically to the real-time runs using archived operational Eta data.

The RAMS model has been successfully used to simulate strongly forced conditions with high snowfall in the Colorado Rocky Mountains (Poulos et al. 2002). One of the advantages of RAMS over other mesoscale and regional-scale models is its representation of microphysics and precipitation processes. As described in Cotton et al. (2003), the microphysics in RAMS follows a new paradigm in cloud parameterization. The model emulates ''binned'' microphysics, including stochastic collection, sedimentation, and activation of cloud-nucleating aerosols, using a number of basis functions in which one to two moments are predicted. As far as mixed- or ice-phase clouds are concerned, the model includes pure vapor-grown ice crystals with a number of temperature-dependent habits, lightly rimed vapor grown crystals called snow, aggregates, graupel, and hail particles. The concentrations of ice crystals are determined from nucleation by vapor deposition or condensation-freezing and by contact nucleation using formulas described by Meyers et al. (1992) or from measurements obtained with continuous flow diffusion chambers from field campaigns. In addition, secondary

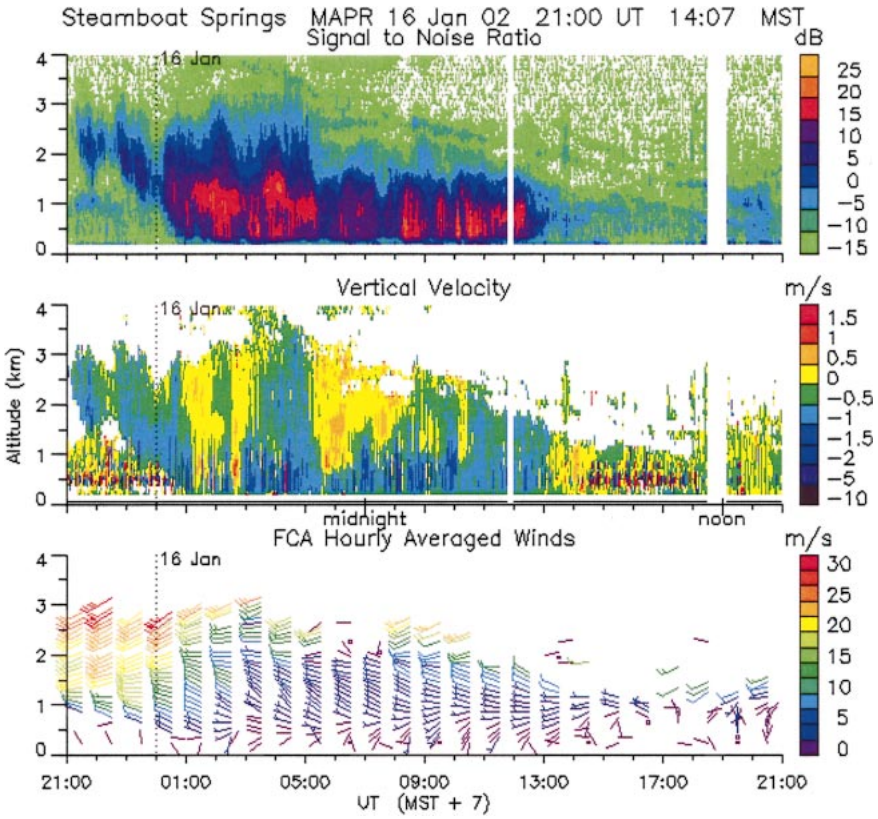

FIG. 11. NCAR MAPR radar profiles of (top) reflectivity SNR (related to precipitation intensity), (middle) vertical velocity (positive upward), and (bottom) horizontal winds for the period 2100 UTC 15 Jan–2100 UTC 16 Jan 2002.

nucleation by the rime-splinter process is parameterized based on data reported by Mossop (1978). This sophisticated physics is accomplished in RAMS without adding a great deal of computational costs by use of lookup tables. Snowfall accumulation is represented as SWE vertical flux. A conversion between snow water equivalent and snow depth is not used operationally. The parameterization of Liston and Pielke (2000) has been applied in some previous studies, but this treatment is valid only for aged snow and not appropriate for the new snow accumulations evaluated in this study. The results of the present study provide new information on parameterization methods useful during snow events in mountainous environments.

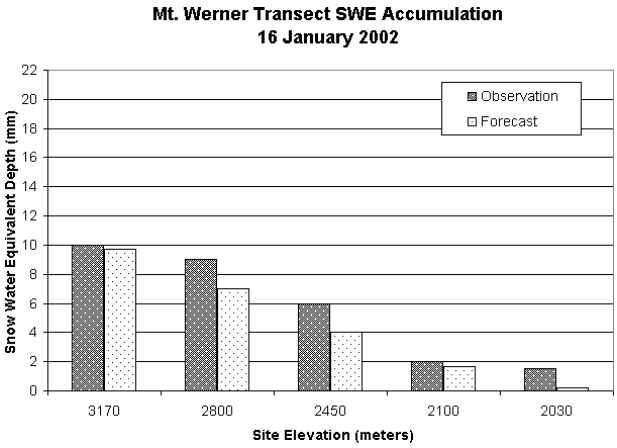

FIG. 12. Elevation comparison of observed and RAMS forecast snow water accumulations for 16 Jan 2002.

3. Forecasting tools for mountainous terrain

Methods for improving snowfall forecasts in radar-limited mountainous terrain are demonstrated in this paper and include identification of key meteorological elements for common event scenarios, use of mesoscale model accuracy in predicting the evolution of these events (even when radar data continues to indicate no precipitation during the event), knowledge of local snowfall climatology, incorporation of improved observational data from precipitation sensor and other meteorological instrumentation at high-elevation sites, and application of satellite data to short-term forecasting and trend analysis.

An empirical relationship commonly used to estimate snow depth from model-predicted precipitation water flux is the observed decrease in snow density as ambient

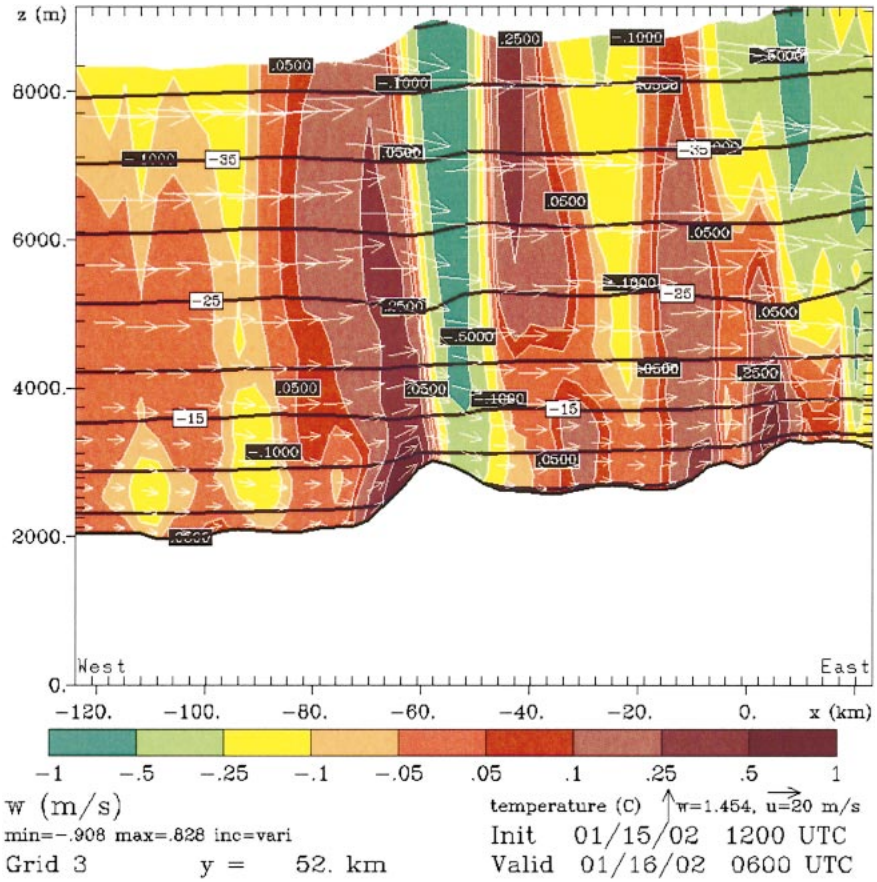

FIG. 13. RAMS model forecast west–east cross section of vertical velocity (color shading), temperature (black contour lines), and airflow vectors for 0600 UTC 16 Jan 2002.

air temperature decreases. A local climatology for winter snowfall density was created for use in the Park Range. Figure 4 presents a time series of total snow depth accumulations during snowfall events (with start and end times determined from visual and gauge data) that were measured at multiple elevations during January and February 2002, and Fig. 5 depicts the snow densities for these samples. The measurements from individual storm events and the period-average values shown at the right-hand end of the chart indicate that most event densities and average snow densities were quite low, with characteristics of greater densities at the lower elevations and increasing density with progression of the season from midwinter. The altitudinal gradients and seasonal tendencies are likely associated with the temperature dependence and mixed-phase growth mechanisms observed in these orographic systems. Measurements made earlier in the season might be expected to show a decrease in snow density from late fall toward midwinter due to airmass characteristics.

A comparison of near-surface (4 m above snow surface) air temperature and new snow density for the three highest-elevation sampling sites during snow events in January, February, and December 2002 is shown in Fig. 6. Air temperatures during the period of maximum snow accumulation along the ridge top were obtained from the SSRC meteorological network and sensors at PHQ and SPL. A linear fit to the data yields the following relationship between density (D) and air temperature (T): $D(\text{g cm}^{-3}) = 0.16 + 0.008\ T\ (^{\circ}\text{C})$, where T is the average air temperature during the period of major snowfall. This equation explains 52% of the variance for the dataset used. A similar degree of correlation was found by previous studies in the same mountainous region (Judson and Doesken 2000). For comparison, also shown in this figure are the data values from a table often applied in NWS operations (NOAA 1997) to estimate new snow density using local air temperature. A second method used by forecasters is the ''10 to 1'' rule (i.e., the density of falling snow is always assumed to be 10% the density of water, or 0.1 g cm^{-3}). The data shown in Fig. 6 indicate that the NWS ''New Snowfall to Meltwater Conversion Table'' (NOAA 1997) would underestimate the density of new snow and that the 10:1 rule is also not representative.

The temperature–density equation derived from local sampling is likely strengthened by the fact that the air temperatures sampled at high-elevation sites are close

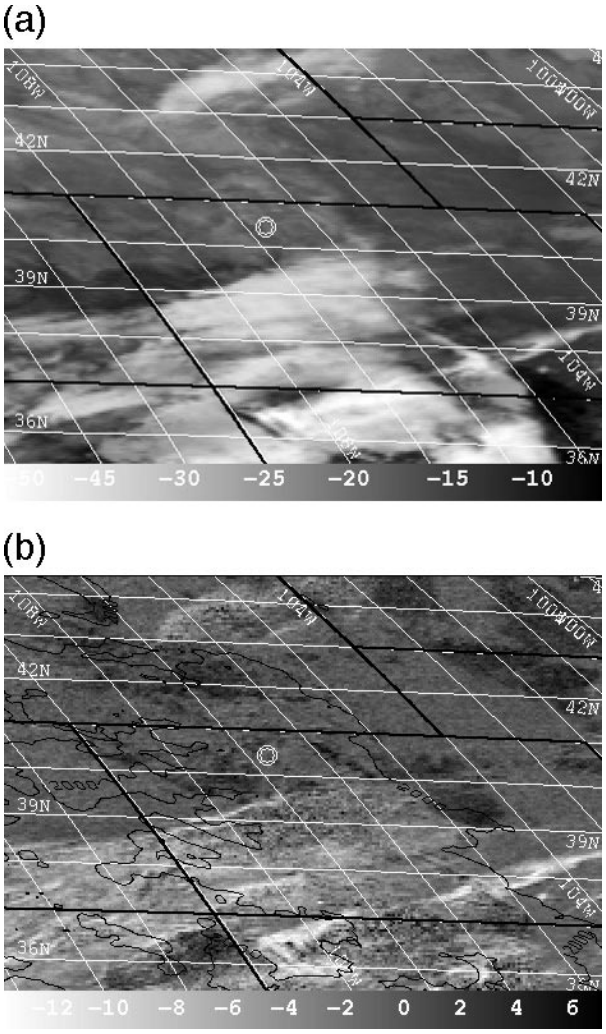

FIG. 14. (a) GOES infrared image at 0800 UTC 16 Jan 2002 with graphic overlay of lat/lon grid lines, state outlines (black), and location of SPL (circle). The grayscale indicates values of equivalent temperature (°C). (b) GOES brightness temperature difference image (11 − 3.9 μm difference) at 0800 UTC 16 Jan 2002 with graphic overlay of lat/lon grid lines, state outlines, topographic contour of 2000-m elevation, and location of SPL (circle). The grayscale indicates values of the brightness temperature differences (°C).

to the temperatures of primary snow growth. Research reported by Kyle and Wesley (1997), using an example of snow falling through a temperature inversion, indicated that the air temperature in the zone of primary snow growth was more directly related to snow density than the surface air temperature. Other factors that can cause variability in an empirically derived relationship between temperature and snow density include the complexity of mesoscale flow fields and cloud microphysical processes in orographic winter storms, and the difficulty in collecting snow survey data immediately following snowfall events. The density–temperature relationships discussed above were applied in the analysis as described in section 4.

Acoustic snow depth gauges can be installed with relatively low cost at mountain sites and are important sources of verification and short-term forecasting information. The SSRC operates an acoustic snow depth sensor at the Patrol Headquarters site (PHQ) on the ridge, and these data are accessed in real time by modem by local site managers. The instruments are located in a clearing of trees to allow protection from wind bias. An antifreeze-type recording tipping-bucket precipitation gauge is operated next to the acoustic sensor. Time series of measurements from these two instruments (Fig. 7) were valuable in determining the SWE and physical snow depth accumulation rates at high elevation (3170 m MSL at this site) and were used in model verification. The RAMS model output used for this study was modified to produce real-time graphics of predicted time series of snow accumulation at specific grid points, and the gridpoint locations were tailored to match available measurement locations. The simultaneous snow depth and snow water time series also permit concurrent analysis of new snow density (Fig. 8). These density estimates are similar to measurements taken manually by the snow survey samples obtained at the same location. For example, all measurements of density during this data period were <0.09 g cm^{-3} except for a high-density period on the morning of day 352, and manual sampling on that morning indicated density of 0.135 g cm^{-3} in the upper 8 cm of the accumulated snow. The snow event on day 352 provided very rapid accumulation, which can create errors in traditional gauge measurements due to snow piling up on the gauge perimeter and then falling into the gauge en masse. When using data from acoustic sensors, it is also important to filter the data for the effects of snow settling, which produces dimishment in snow depth between snowfall events (Labine 1996). Settling effects can also progress during snowfall, particularly if air temperature increases rapidly.

One of the most valuable methods of improving short-term weather prediction in mountainous terrain is to more fully incorporate point data, such as the snowfall and snow density observations, into the interpretation of the current and past few hours of meteorological events, with comparison to and updated interpretation of the available mesoscale model output. While the Park Range suffers from restricted radar coverage, it has the advantage of multiple measurement locations, including SNOTEL sites, a ski area with modem-accessible acoustic snow depth gauge and other observations, and the DRI Storm Peak Laboratory with Web-accessible meteorological time series. This type of instrumentation and data access allow point validation of mesoscale model forecasts and evaluation of model performance that can aid interpretation of the ongoing event as well as provide the forecaster with improved composite knowledge of model biases under different event scenarios.

Ongoing advancement of local forecasting in moun-

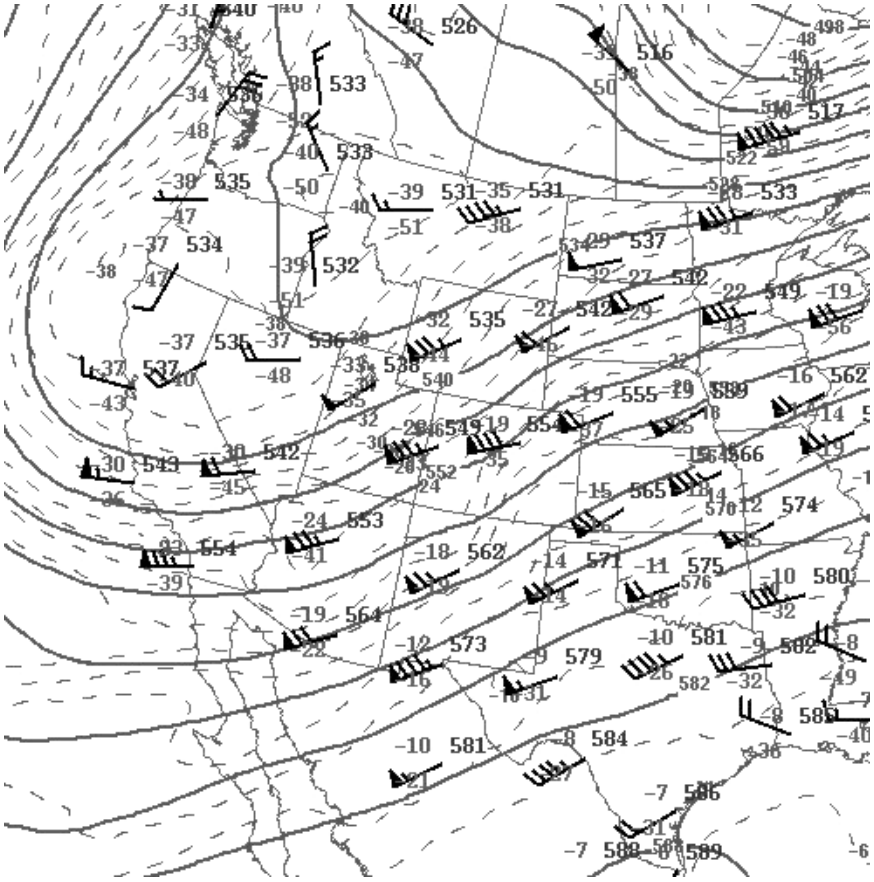

FIG. 15. As in Fig. 9 except for 0000 UTC 29 Jan 2002.

tainous areas can take advantage of improved model resolution that more fully resolves complex terrain. As each model improvement is made, however, a new learning curve is imposed on the forecasters, and previous model biases may be mistakenly accommodated and new biases combined to increase forecast error. It is therefore important to carry out case studies of snowfall events that represent characteristic types of synoptic evolution in the locale. This study uses three typical orographic snowfall events for the purpose of evaluating model performance and implementing additional forecast tools such as use of snow density–air temperature relationships, satellite data analysis, and increased use of surface measurements.

4. Implementation for case study analysis

Specific weather events are presented to demonstrate methods for improving the short-term prediction of snowfall accumulation over radar limited-signal terrain. The results provide information on the overall performance of the RAMS 3-km-grid mesoscale model, including forecasting QPF with differing winter storm events. The results also focus on incorporating, in an operational setting, routine available observations and model output, such as the RAMS, to enhance snowfall forecasting and verification in mountainous areas.

a. Westerly upslope flow

This event was known as a ''champagne powder day'' for the Steamboat Springs ski resort. While events of low-density snow and associated rapid accumulation of snow depth are common during midwinter in the Park Range, the ability to identify the intensity of these events is hampered by the lack of radar signal in the area. Key meteorological elements for this case study include a favorable westerly flow orographic uplift and a combination of moisture and temperature profiles that optimize the Bergeron–Findeisen process for crystal growth.

A positively tilted trough extended across the western United States as indicated by the 500-hPa height analysis at 0000 UTC 16 January 2002 (Fig. 9). A series of weak short waves in association with the main trough moved across northern Colorado during the morning hours of 16 January. Model cross-sections (not shown) from the 0000 UTC 16 January Eta model run for Steamboat Springs indicated weak instability through 0600 UTC 16 January, adequate moisture (≥80% rel-

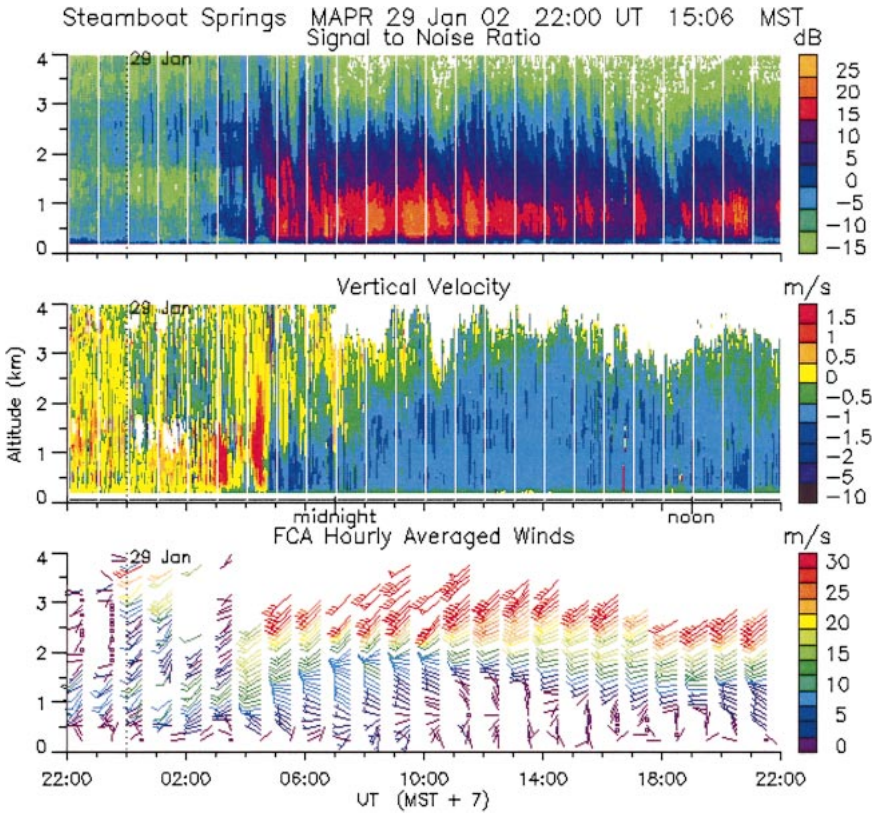

FIG. 16. As in Fig. 11 except for the period 2200 UTC 28 Jan–2200 UTC 29 Jan 2002.

ative humidity up to 600 hPa), and a west flow (15 kt) at 700 hPa. The upper-level water vapor and cloud-top temperature distributions obtained from satellite imagery indicated a large area of subtropical moisture advecting across the southwestern portion of the United States. A 50+ m s^{-1} (100–120 kt) jet at 300 hPa sustained the moisture feed ahead of the trough. With modest moisture and upslope, the Grand Junction Weather Forecast Office (GJT-WFO) 15 January afternoon forecast called for 2–5 cm of snow accumulations over lower elevations around the town of Steamboat Springs with 7–15 cm over higher elevations in the Park Range.

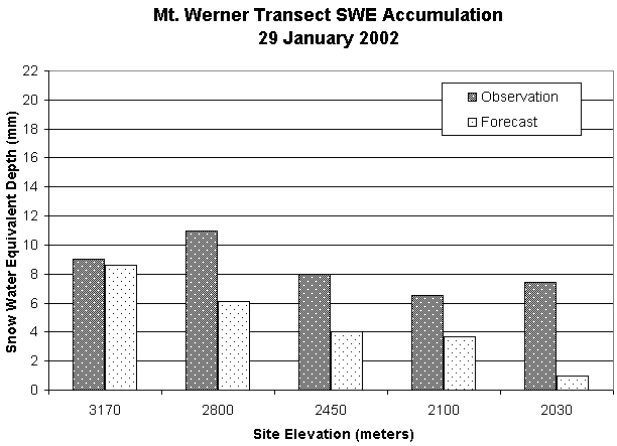

FIG. 17. Elevation comparison of observed and RAMS model forecast snow water accumulations for 29 Jan 2002.

Upward vertical velocity in the 700–400-hPa layer, combined with favorable upslope flow in a fairly moist regime, generated a large elevation gradient of snowfall amounts across the Park Range by 1200 UTC 16 January. Snow amounts increased markedly from the town of Steamboat Springs, which received only 2 cm snowfall to the ridge-top location where 32 cm accumulated snowfall was measured, which exceeded GJT-WFO forecasted snowfall amounts for the Park Range. The RAMS predicted maximum precipitation rates (1.5–2.5 mm h^{-1}) in the central Park Range to occur in a narrow time window centered on 0400 UTC (Fig. 10). Precipitation gauge measurements at the MAPR site, located near the base of the Park Range near Steamboat Springs, also show that the primary pulses of snowfall in the central portion of the Park Range occurred between 0200 and 0600 UTC. Figure 11 is a time series of data parameters obtained from the MAPR radar. The radar reflectivity signal-to-noise ratio (SNR) profiles represent the intensity of precipitation through the echo region, with the most intense precipitation during 0200–0500 UTC. Additional shallow precipitation is indicated during 0800–1200 UTC. The reflectivity increases beginning at 0000 UTC 16 January, diminishes at 0600 UTC,

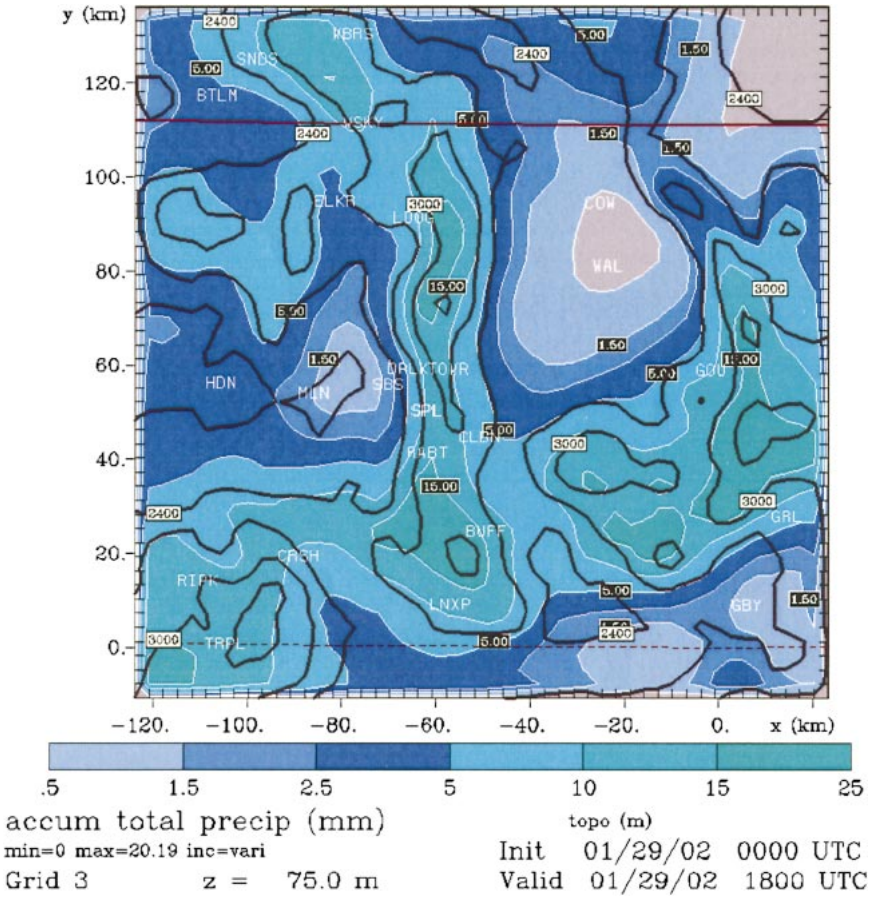

FIG. 18. RAMS model forecast of accumulated precipitation (color shading) for the period 0000–1800 UTC 29 Jan 2002 overlaid with model topography (m) (black contour lines).

and tapers off to background echo signal levels by 1400 UTC. The periods of maximum reflectivity correspond to the strongest west flow. The MAPR vertical velocities are indicative of snowfall rate, and horizontal wind profiles provide information on wind velocities and shear. A temporal change from strong southwest flow to moderate northwest flow, seen in the MAPR profiles just above ridge level (1.7–1.9 km AGL) over the period 0000–0800 UTC, was associated with a shift in the zone of maximum orographic precipitation from the northern Park Range early, to the central and southern portions of the range in later hours.

Figure 12 depicts a comparison of SWE depths measured at five snow survey sites along an elevation transect, extending from 7 km west of Steamboat Springs to the ridge top, and QPF (accumulated SWE) predicted by the RAMS forecast model for those locations. Model values of SWE were bilinearly interpolated from four 3-km grid points surrounding each site location. The sampling transect points are spaced closely enough that they are sequentially separated by just one or two model grid points. The RAMS model predicts snowfall rate in terms of water-equivalent flux (rather than snow depth accumulation rate), so SWE values are compared. The accumulation period and ending time for the model output was selected to match the snow sampling time at each site. In this case, the verification periods for the SWE total accumulation were 22.0–29.5 h (depending on sample site location) after the model initialization at 1200 UTC 15 January.

The RAMS SWE forecast matched that of the observation (10 mm) at the highest-elevation sampling location, but the model underpredicted SWE at the lower elevations. If the temperature–density relationship presented in section 3 were used, the predicted snowfall accumulations for the higher-elevation zone of the Park Range would likely have been high enough to issue a ''winter storm warning'' (greater than 30 cm of snowfall). However, the RAMS model predicted temperatures in the cloud layer approximately 5°C warmer than observed by rawinsonde and surface measurements, which may impact the simulation of the moist adiabatic processes during forced orographic ascent. The model topography smoothed to a 3-km grid creates ridge-top surface elevations in the model that are on the order of 500 m lower than the actual envelope of the mountain range. A method to more adequately simulate orographically forced cloud processes is to use a ''silhouette''

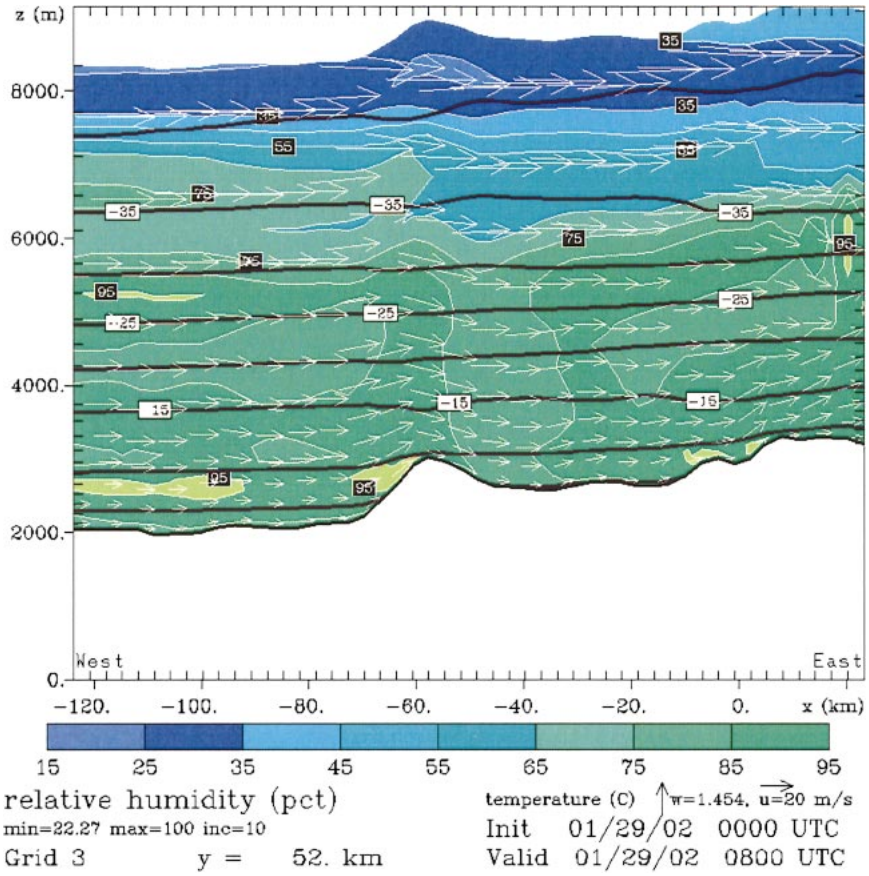

FIG. 19. RAMS model-predicted cross section of relative humidity (color shading), temperature (black contour lines), and airflow vectors for 0800 UTC 29 Jan 2002.

topography that applies the maximum elevation data available (from the 30-s data in this case) to all model grid cells where elevations occur over a certain value (such as 3 km).

A number of other aspects of the RAMS model forecast accuracy can be demonstrated using the available measurement data. Cloud base was estimated from the GLASS profiles and the SSRC mesonet data to be ~ -5°C and 2100 m MSL (significantly below the ridgetop level). This corresponds to the model temperature distribution shown in a 0600 UTC west–east cross section (Fig. 13). The cross-section data are for the north–south coordinate line of $y = 52$ km in the grid 3 domain (Fig. 3b). The limited temperature range of the cloud layer and the westerly flow profiles that promoted orographic uplift in the central Park Range allowed very efficient snow production. The model cross section depicts uplift directly upwind of SPL at temperatures near -15°C, a temperature regime conducive to diffusional snow growth. Ice crystals observed at SPL during the early period of snowfall were broadly branched dendrites with light to moderate riming at concentrations <10 L^{-1}, mixed with cloud droplets with average diameter 10 μm and number concentrations 580 cm^{-3}. The temperature regime allowed efficient evaporation of droplets and diffusional growth of crystals via the Bergeron process. At the same time, relatively high concentrations and small sizes of cloud droplets indicated conditions where the availability of aerosol reduced the droplet-to-crystal collection efficiency, thus suppressing riming growth and snow density (Borys et al. 2003). As the snowfall period progressed further, the crystals were predominantly unrimed dendrites, and the microphysical observations suggest that the cloud water was consumed by the diffusion-dominated crystal growth process. Microphysics data confirmed RAMS model forecasts that supercooled cloud water was not present over the mountain range after 0800 UTC.

Additional information on snow growth processes in orographic clouds can be obtained from satellite data analysis, including the use of quantitative parameters to characterize cloud microphysical structure and time-lapse animations to indicate cloud layer evolution (Wetzel 1995; Rosenfeld and Gutman 1997). Deep ice cloud covered the study region in the early hours of the precipitation event, but during the period that produced very low density snow, the upper-level cirrus had moved away from the area and local cloud tops were at mid-

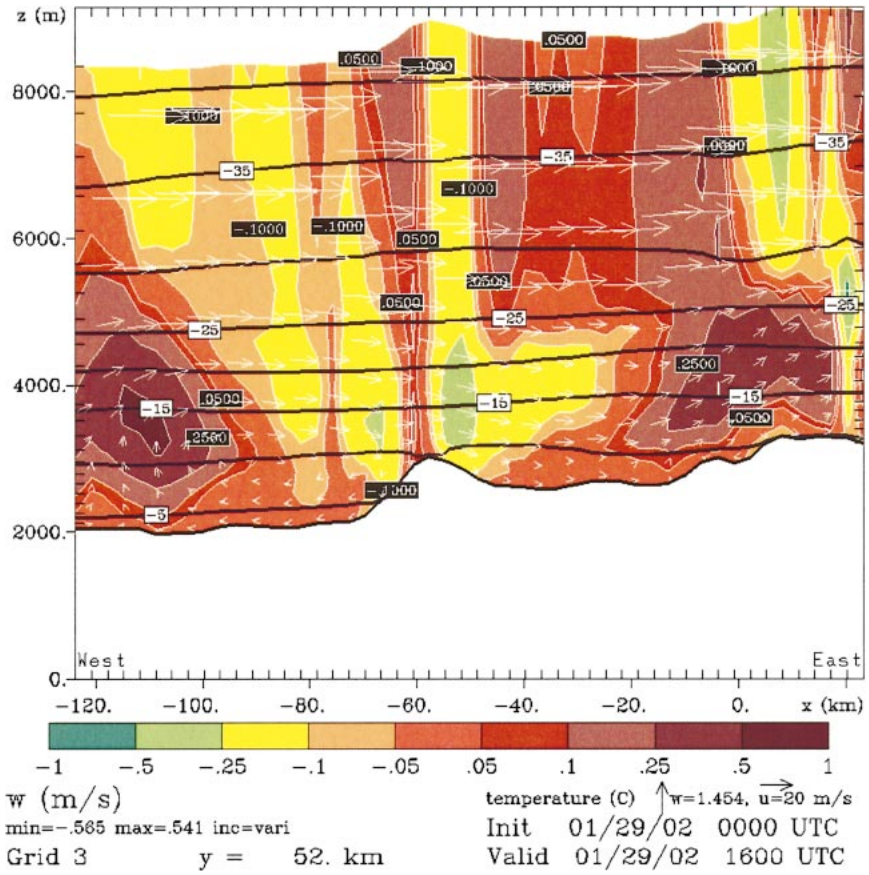

FIG. 20. RAMS model forecast of vertical velocity (color shading), temperature (black contour lines), and airflow vectors for 1600 UTC 29 Jan 2002.

levels. Cloud-top temperatures observed in the IR imagery were −20°C to −23°C during the period of maximum snowfall accumulation, and GLASS profiles indicated cloud top near −25°C (5100 m MSL). Satellite digital image data were used to calculate the difference between equivalent cloud-top temperatures in the GOES infrared (IR) and near-infrared (NIR; 3.9-μm channel) images. This $T_{IR} - T_{NIR}$ brightness temperature difference (BTD) at night is typically negative for cloud that is primarily composed of ice crystals at cloud top, and near zero or slightly positive for mixed-phase or water cloud (Baum et al. 1994). Figures 14a and 14b present a pair of GOES images at 0800 UTC for the infrared and the brightness temperature difference, respectively. The infrared brightness temperatures (Fig. 14a) of the orographic cloud over SPL (position indicated by the circle) were −20° to −23°C, while over the cold cloud shield to the south these temperatures were colder than −40°C. Sampling of data from the corresponding image for the brightness temperature difference (Fig. 14b) indicated values of BTD predominantly in the range −3° to −7°C for the cold cloud shield, while BTD values over SPL were in the range −0.2° to 2.5°C. A time series of IR images and BTD data indicated that the cirrus shield had moved southward from the study location after 0200 UTC, revealing a view of cloud tops with BTD values that suggest a mixed-phase cloud during the time of maximum accumulation of low-density snowfall, followed by glaciation and then dissipation of the cloud. Satellite multispectral imagery is valuable for identification of shallow, supercooled cloud layers, determination of cloud-top glaciation, and validation for mesoscale model predictions of orographic cloud structure.

b. Southwest blocking and airflow decoupling

A broad positively tilted trough extended over the western United States at 0000 UTC 29 January 2002 as denoted by the 500-hPa height analysis shown in Fig. 15. Strong southwest flow ahead of this system was situated over north-central Colorado, with a 75 m s^{-1} (150 kt) jet core at 250 hPa by 0000 UTC 29 January. In addition, a slow-moving baroclinic zone and associated surface cold front moved across northwest Colorado between 0000 and 1200 UTC 29 January. The environment ahead of the cold front was unstable with a lifted index of −1, taken from the 0000 UTC 29

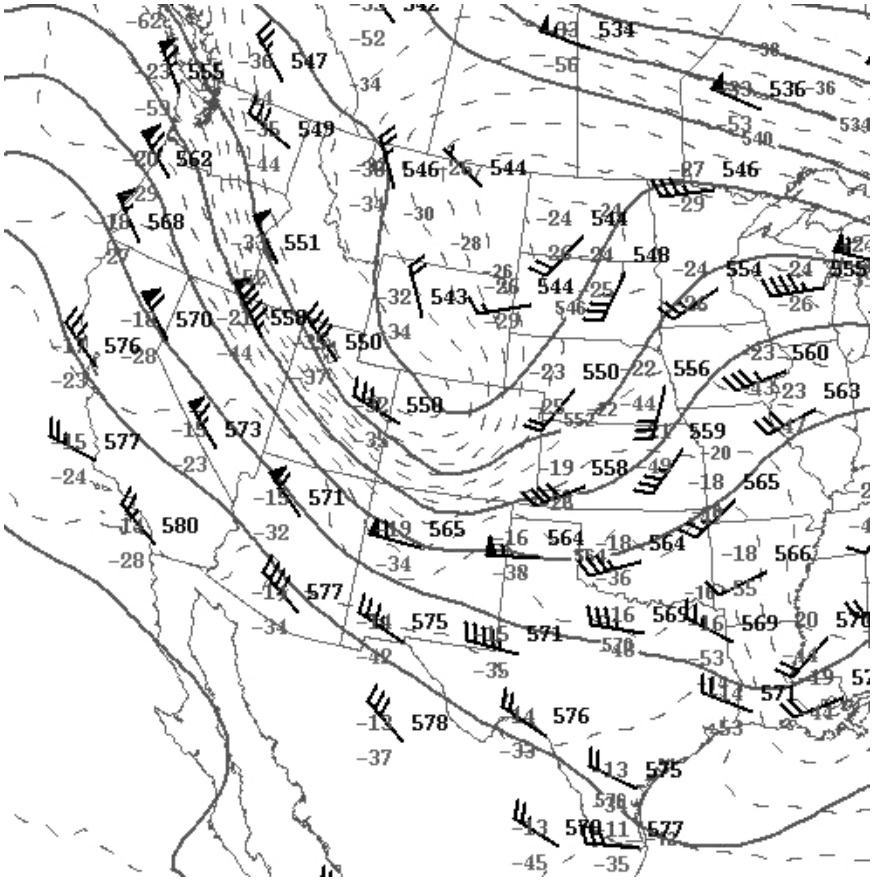

FIG. 21. As in Fig. 9 except for 0000 UTC 9 Feb 2002.

January sounding at GJT-WFO. Behind the cold front, the air mass was moist, with relative humidity >80% up to 550 hPa, and low-level winds were westerly. At 700 hPa, temperatures fell from −8° to −14°C between 0000 and 1200 UTC 29 January, keeping the air mass nearly moist adiabatic below 550 hPa over the Park Range.

As the trough moved east from the California coast toward the desert southwest, the 500-hPa flow became more southerly and slowed the progression of the thermal gradient over northwest Colorado. With winds parallel to the thermal gradient, upward lift associated with several embedded disturbances moved across north-central Colorado, enhancing the potential for significant snowfall. Southwest flow typically does not produce significant snowfall over the Park Range, primarily because it is located to the lee of the Flat Tops Plateau in west-central Colorado (~3600 m MSL), and a mountain ''precipitation shadow'' effect typically prevails. However, the slow-moving baroclinic zone and very strong winds aloft generated significant upward vertical motion, which overcame this mountain shadow effect. The air mass stabilized over the Park Range after 0000 UTC 30 January. For the their afternoon issuance on 28 January, GJT-WFO forecasted 30–60 cm at elevations above ~2750 m (9000 ft) in the Park Range and 15–30 cm below 2750 m MSL for total storm accumulation, for a period that extended through the morning of 30 January. In the vicinity of Steamboat Springs, 10–20 cm of snow was predicted. Measured snow accumulation (Fig. 4) at the Patrol Headquarters site (PHQ; 3170 m) was 20 cm for 29 January and 22 cm for 30 January, with the lower-elevation sampling sites receiving 15–20 cm for the 2-day period.

The strength and moisture content of the airflow during this event was sufficient to produce snowfall in this southwest flow regime (Fig. 16). The flow became decoupled and convergence in the midmountain elevation zone (see wind profile near 1000 UTC in Fig. 16) may have enhanced SWE capture below the ridge top as observed for January 29 (Fig. 17), and contributed to the wide distribution of snowfall over the entire region (Fig. 18). The less favorable orographic component due to southwest flow may also have reduced the elevational gradient in snowfall. A broad coverage of significant snowfall amounts across the area at middle and lower elevations was evident in the model simulations.

The RAMS model forecast (Fig. 19) indicated relatively warm temperatures (>−15°C) at levels above the mountain ridge (~3800 m). Time series measurements

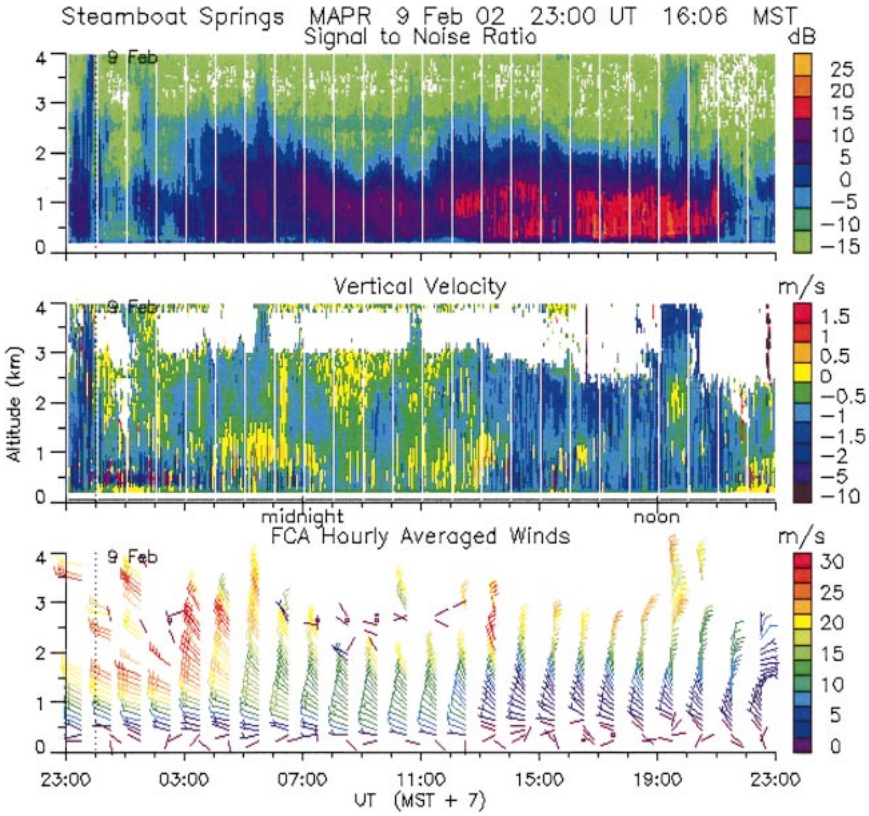

FIG. 22. As in Fig. 11 except for the period 2300 UTC 8 Feb–2300 UTC 9 Feb 2002.

at SPL provide evidence that the model overpredicted air temperature during the snow event, as in the 16 January case. The magnitude of the cooling trend from 0000 to 1500 UTC on 29 January for SPL was forecast to be 5°C rather than the 10°C cooling observed at the elevation of ridge top. This would cause higher estimates of snow density and thus underprediction of snow depth accumulations, particularly with the model underprediction of snow mass flux at lower elevations (Fig. 17). A more accurate (colder) forecast air temperature at ridge top would have led to decreased estimates of snow density and increased snow depth predictions. The timing of the model-simulated temperature minimum (approximately 1500 UTC) did agree with observations. The later portion of the snow event (near 1600 UTC) with airflow decoupling is evident in both the MAPR data (Fig. 16) and the RAMS model forecast (Fig. 20), and the model data also indicated downward motion to the west of the Park and Gore Ranges. The overall analysis of the model simulations suggests good performance in predicting the structure of this storm, during a period of highly dynamic evolution and observations that indicated instability and strong upper-level forcing.

c. Wraparound northwest flow

An open wave trough was located over the central Rockies as indicated by the 500-hPa height analysis at 0000 UTC 9 February 2002 (Fig. 21). By 1200 UTC 9 February the main trough had moved east and deepened over western Kansas. Upper-level lift between 700 and 400 hPa associated with weak short waves wrapping around the closed low combined with strong orographic lift, enhanced snowfall amounts during the daytime hours on 9 February. An Eta model time–height cross section over Steamboat Springs indicated relatively shallow moisture with this system, with relatively humidity of >80% found below 600 hPa, after 1500 UTC on 9 February. This system was also characterized by strong northwest flow, as evidenced by the 700-hPa analysis of ≥30 kt and relatively cold temperatures (~−15°C) at 1800 UTC. As the system moved east into the central Plains, precipitation ended by 0200 UTC. Given the limited moisture, GJT-WFO issued a forecast in the afternoon of 8 February for 10–20 cm of snow for the Park Range, with only light accumulations for the town of Steamboat Springs.

A combination of upper-level lift associated with a series of midlevel short waves (0300–2000 UTC during 9 February), orographic uplift due to strong northwest flow, and unstable lapse rate during the daytime hours led to extended precipitation (Fig. 22). Snow began to fall across the Steamboat Springs area at 0300 UTC 9 February and continued through the following evening.

The primary snow accumulation predicted by the

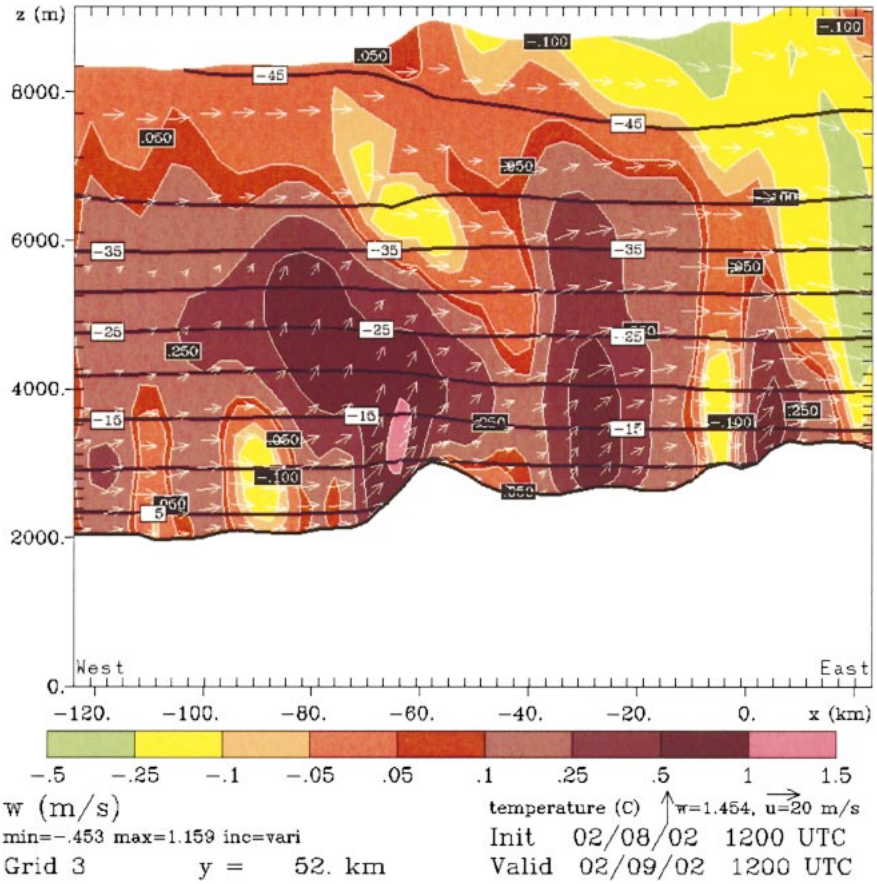

FIG. 23. RAMS model forecast cross section of vertical velocity (color shading), temperature (black contour lines), and airflow vectors at 1200 UTC 9 Feb 2002.

RAMS simulations occurred beginning 1200 UTC 9 February, during the strongest period of northwest flow at ridge-top level that was accompanied by deep upward vertical velocities (Fig. 23) and condensate production (Fig. 24). Winds measured at SPL verified the favorable northwest flow pattern (Fig. 25). The termination of precipitation occurred near 2300 UTC 9 February, when winds at the barrier level increased (see Fig. 22).

The Grand Mesa, Colorado (GJX), WSR-88D radar reflectivity (Fig. 26) indicated no precipitation occurring over the mountain locations around Steamboat Springs. The combination of distance from the GJX radar origin and topographic beam blockage often causes a lack of radar signature for precipitation in the Yampa Valley region. During this time period, significant precipitation over the region was forecast by RAMS (Fig. 27) and was verified. RAMS forecast accumulations in the upper zone of the Park Range were similar to observed (Fig. 28), and the mesoscale model forecast provided a better representation of the storm evolution than radar observations revealed. However, more snow fell into the lower-elevation zone than was predicted by the model. As in the previous two cases, the model forecast air temperatures were warmer than measured near ridge top during the precipitation period. This can influence the model microphysical processes and also can cause a low estimate of accumulated snow depth when forecast air temperature and mass flux are used to estimate the density of falling snow. The results suggest that improvements in the model forecast temperatures, and the use of real-time measurement sites at higher elevations to track observed temperature trends, especially in radar signal-limited terrain, could increase the accuracy of short-term predictions for snow depth.

5. Discussion and conclusions

Radar detection of snowfall is limited in many mountainous regions, so the combined use of model forecasts and other available observations becomes essential to prediction and verification of precipitation distribution. This study demonstrated techniques to more fully apply observations and mesoscale models in analysis of orographic snowfall. Ridge-top predictions of snow accumulation and timing were evaluated for three winter events in the Park Range of northwest Colorado. To demonstrate a procedure that can be used for real-time intercomparison of observations and model output,

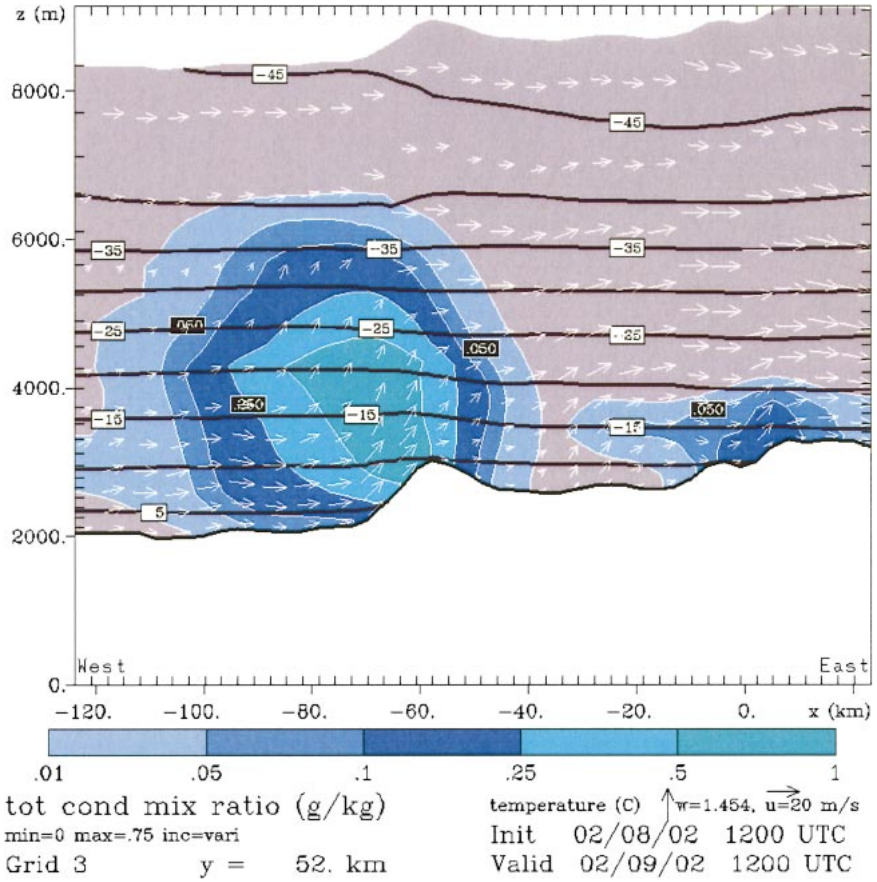

FIG. 24. RAMS model forecast of condensate (cloud + snow) mixing ratio (color shading), temperature (black contour lines), and airflow vectors at 1200 UTC 9 Feb 2002.

model values of SWE were bilinearly interpolated from the four 3-km grid points surrounding locations at which snow sensor measurement data were available. The precipitation distribution as forecast by the RAMS mesoscale model was very similar to observed snow water equivalent values near ridge top, but there was a tendency for underprediction at lower elevations. Most forecast models provide QPF parameters for snow in terms of water equivalent rather than snow depth, because of the difficulties in estimating the density of snowfall. Therefore, accurate forecasts of snow water equivalent as well as a method for estimating snow density are needed for the region of interest. Field measurements of several snow events in the study region have been combined to obtain an empirical relationship between air temperature and snow density in the typical elevation zone of precipitation for this mountain ridge that could be applied to model output (of SWE) to estimate snow depth. This dataset is specific to the region and typical cloud structure on the Park Range and provides a useful tool for estimating snow density in this region of the Rocky Mountains.

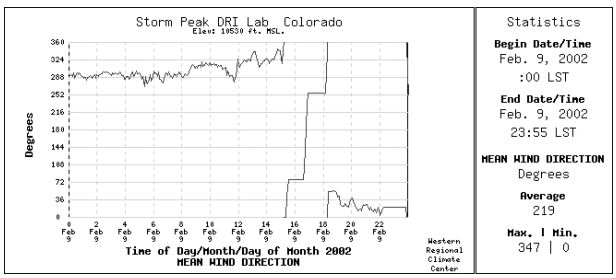

FIG. 25. Time series of wind direction measured at SPL on 9 Feb 2002 (LST = UTC − 7h).

This study also demonstrated real-time estimation of snow density using snow water and acoustic snow depth measurements at high temporal resolution, and the application of snow survey transect data for model verification. Agreements with organizations such as transportation departments and ski areas can be established to obtain valuable snow depth and density information. In orographic cloud systems, snow growth is most likely to be maximized near cloud base along mountain slopes and ridges, so information on snowfall, temperatures, and winds is needed at high-elevation sites. An example of data acquisition at a ski area is used in this study. In operational application, NWS forecast offices could in-

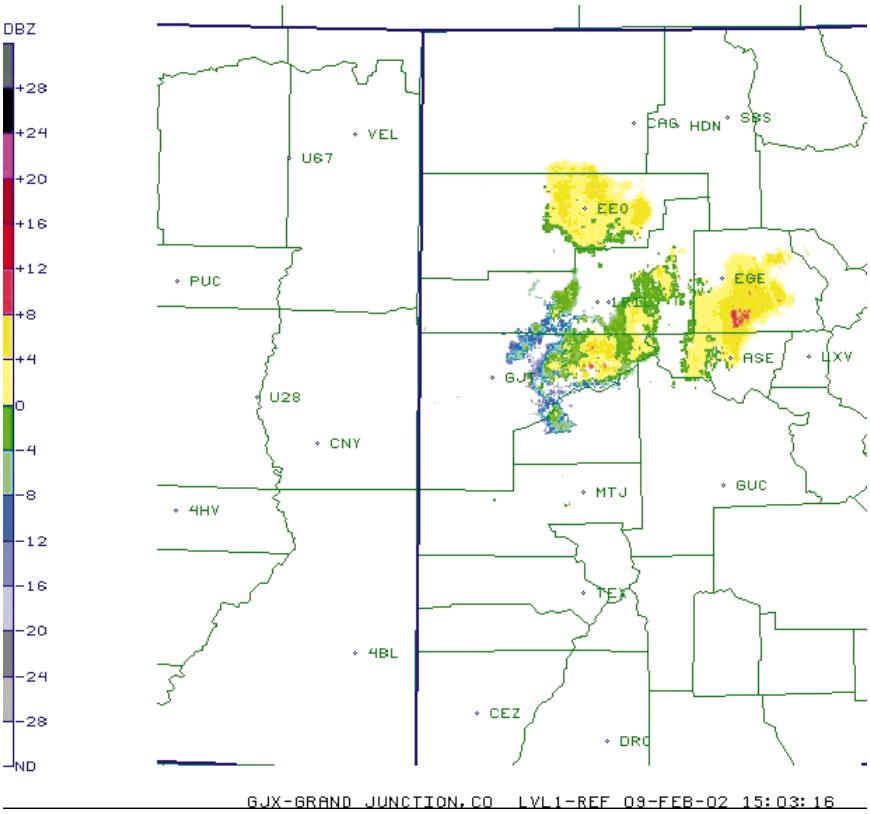

FIG. 26. NWS Grand Mesa, CO (GJX), radar reflectivity (dBz) scan for 1509 UTC 9 Feb 2002. The scan does not reveal the snowfall occurring over the area of Steamboat Springs (SBS) and Park Range (as indicated in Fig. 21). County lines and station identifiers are indicated in green; state lines are blue.

crease recruitment and training of cooperative weather ''spotters'' and make agreements with local ski areas, transportation departments, or other organizations to obtain point-specific measurements of snow depth and snow water equivalent in mountainous regions. These data would enhance the value of data from the National Resources Data Network (NRCS) SNOTEL network (http://www.wrcc.dri.edu/snotel.html) and would contribute to real-time analysis and climatological summary of snow density characteristics in differing snowfall regimes. The MesoWest network of observational sites (http://www.met.utah.edu/mesowest) is a valuable source of real-time access to a large array of parameters related to winter weather, and a significant effort has been made in Utah to facilitate public access to measurements related to snowfall. The U.S. Forest Service (USFS)–Bureau of Land Management (BLM) Remote Automated Weather Station (RAWS) network provides near-real-time and archived time series of wind, temperature, solar radiation, and other meteorological parameters useful in winter weather analysis. The RAWS network includes hundreds of sites, including a large number in mountainous western states (http://www.raws.dri.edu/index.html). There are also data available from an increasing number of high-altitude measurement sites established for transportation monitoring activities. For example, Automated Weather Observing System (AWOS) sites have been installed by the Colorado Department of Transportation at several mountain pass locations (http://www.Colorado-Aeronautics.org/aeroawos.htm) to aid both aviation and highway transportation. Real-time interpretation of mountain-sited observations, applied in conjunction with tailored products from mesoscale models and case study examples of orographic effects, will lead to improvements in the quantitative forecasting of snowfall distribution. With the advent of the NWS National Digital Forecast Database, new opportunities and imperatives exist for the incorporation of point measurement and elevation-specific local climatological data into the forecast preparation procedures.

The case study analyses indicated that though the operational forecasts of snow depth accumulation could be improved through the use of SWE forecasts and temperature–density relationships, further improvement is needed for the model simulation of air temperature vertical distribution. In particular, it was evident that the model overestimated air temperature in the zone of mixed-phase precipitation growth, and that the use of a smoothed grid elevation dataset contributes to warm

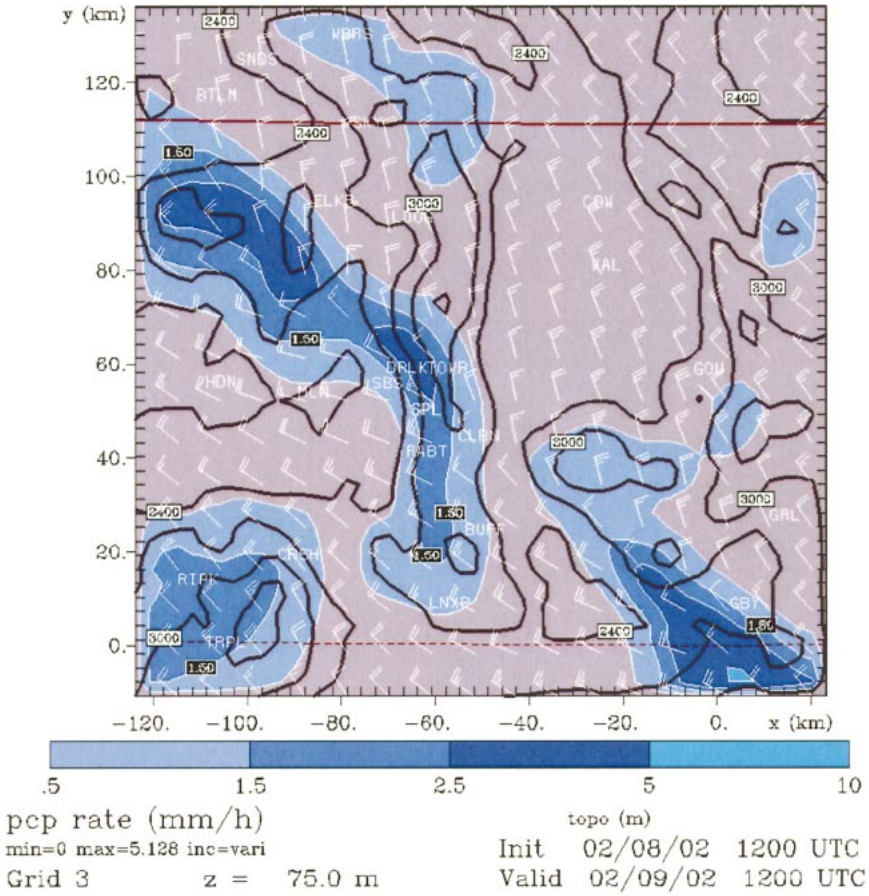

FIG. 27. RAMS model forecast of precipitation rate (color shading) overlaid with model topography (m) (black contour lines) at 1200 UTC 9 Feb 2002.

bias by underrepresenting orographic effects on moist adiabatic processes. A more precise representation of surface topography is planned in future model applications to use the ''silhouette'' of the topography (the highest elevations within the 30-s elevation database for terrain above 3 km) to improve the simulation of orographic effects on moist adiabatic processes during forced ascent over the mountain range. Graphical products for model profiles sited along the topographic cross section of the primary airflow can be used to adjust estimates of adiabatic cooling in parcels lifted across the mountain range. This project utilized a cooperative partnership between NWS and university groups to implement and test a 3-km mesoscale model. Such collaboration is recommended as a very effective way for a NWS forecast office to obtain real-time model simulations that realistically represent the mesoscale dynamics and snow growth environments unique to winter orographic storms.

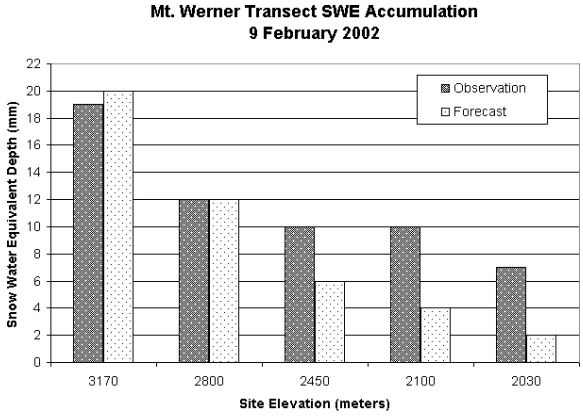

FIG. 28. Elevation comparison of observed and RAMS model forecast snow water accumulations for 9 Feb 2002.

Acknowledgments. Support for this research was provided by the Cooperative Program for Operational Meteorology, Education and Training (COMET) under University Corporation for Atmospheric Research (UCAR) Grants S02-38657 and S00-19126, and by a National Science Foundation (NSF) grant to the Desert Research Institute (DRI) through Grant ATM-0004265. The COMET funding was provided by a cooperative agreement between the National Oceanic and Atmospheric

Administration (NOAA) and UCAR. The views expressed herein are those of the authors and do not necessarily reflect the views of NOAA, its subagencies, or UCAR. Participation by scientists from the National Center for Atmospheric Research (NCAR) was supported by the NSF grant to DRI. NCAR is operated by UCAR under sponsorship of NSF. The authors extend appreciation for manuscript review to Preston Leftwich, National Weather Service Central Region Headquarters. Many thanks to DRI engineers (Rick Purcell, Dan Wermers), NCAR engineers and scientists (including Ned Chamberlain, Mike Susedik, Terry Hock), and the staff of the NWS Grand Junction Forecast Office. Logistical assistance from the Steamboat Ski and Resort Corporation is greatly appreciated. DRI is an equal opportunity service provider and employer and is a permittee of the Medicine-Bow and Routt National Forests.

REFERENCES

Baum, B. A., R. F. Arduini, B. A. Wielicki, P. Minnis, and S.-C. Tsay, 1994: Multilevel cloud retrieval using multispectral HIRS and AVHRR data: Nighttime oceanic analysis. *J. Geophys. Res.,* **99,** 5499–5514.

Borys, R. D., and M. A. Wetzel, 1997: Storm Peak Laboratory: A research, teaching, and service facility for the atmospheric sciences. *Bull. Amer. Meteor. Soc.,* **78,** 2115–2123.

——, D. L. Lowenthal, and D. L. Mitchell, 2000: The relationships among cloud microphysics, chemistry, and precipitation rate in cold mountain clouds. *Atmos. Environ.,* **34,** 2593–2602.

——, D. H. Lowenthal, S. A. Cohn, and W. O. J. Brown, 2003: Mountaintop and radar measurements of aerosol effects on snow growth and snowfall rate. *Geophys. Res. Lett.,* **30,** 1538, doi:10.1029/2002GL016855.

Cohn, S. A., W. O. J. Brown, C. L. Martin, M. S. Susedik, G. MacLean, and D. B. Parsons, 2001: Clear air boundary layer spaced antenna wind measurements with the Multiple Antenna Profiler (MAPR). *Ann. Geophys.,* **19,** 845–854.

Cotton, W. R., and Coauthors, 2003: RAMS 2001: Current status and future directions. *Meteor. Atmos. Phys.,* **82,** 5–29.

Dey, C. H., 1998: Office Note 388, GRIB (edition 1). U.S. Dept. of Commerce, NOAA/NWS/NCEP, 147 pp. [Available online at http://www.nco.ncep.noaa.gov/pmb/docs/on388/download.]

Goodison, B. E., 1978: Accuracy of Canadian snow gage measurements. *J. Appl. Meteor.,* **17,** 1542–1548.

Heggli, M. F., and R. A. Rauber, 1988: The characteristics and evolution of supercooled liquid water in wintertime storms over the Sierra Nevada: A summary of microwave radiometric measurements taken during the Sierra Cooperative Pilot Project. *J. Appl. Meteor.,* **27,** 989–1015.

Judson, A., and N. Doesken, 2000: Density of freshly fallen snow in the central Rocky Mountains. *Bull. Amer. Meteor. Soc.,* **81,** 1577–1587.

Kyle, J. P., and D. A. Wesley, 1997: New conversion table for snowfall to estimated meltwater: Is it appropriate in the High Plains? Central Region ARP 18-04, National Weather Service, Cheyenne, WY, 4 pp.

Labine, C., 1996: Automatic monitoring of snow depth. *Proc. Int. Snow Science Workshop,* Banff, Canada, Canadian Avalanche Centre, 179–183. [Available online at http://www.avalanche.org/~issw/96.]

Li, L., and J. W. Pomeroy, 1996: Estimates of threshold wind speeds for snow transport using meteorological data. *J. Appl. Meteor.,* **36,** 205–213.

Liston, G. E., and R. A. Pielke Sr., 2000: A climate version of the regional atmospheric modeling system. *Theor. Appl. Climate,* **66,** 29–47.

Lowenthal, D. H., R. D. Borys, and M. A. Wetzel, 2002: Aerosol distributions and cloud interactions at a mountaintop laboratory. *J. Geophys. Res.,* **107,** 4345, doi:10.1029/2001JD002046.

Maddox, R. A., J. Zhang, J. J. Gourley, and K. W. Howard, 2002: Weather radar coverage over the contiguous United States. *Wea. Forecasting,* **17,** 927–934.

Magono, C., and C. W. Lee, 1966: Meteorological classification of natural snow crystals. *J. Fac. Sci.,* **7,** 321–362.

Meyers, M. P., and W. R. Cotton, 1992: Evaluation of the potential for wintertime quantitative precipitation forecasting over mountainous terrain with an explicit cloud model. Part I: Two-dimensional sensitivity experiments. *J. Appl. Meteor.,* **31,** 26–50.

——, P. J. DeMott, and W. R. Cotton, 1992: New primary ice-nucleation parameterizations in an explicit cloud model. *J. Appl. Meteor.,* **31,** 708–721.

——, E. M. Page, R. L. McAnnelly, and W. R. Cotton, 2001: Operational fire weather support through the use of a mesoscale forecast model. Preprints, *Ninth Conf. on Mesoscale Processes,* Fort Lauderdale, FL, Amer. Meteor. Soc., 234–235.

Mossop, S. C., 1978: The influence of drop size distribution on the production of secondary ice particles during graupel growth. *Quart. J. Roy. Meteor. Soc.,* **104,** 323–330.

NOAA, 1997: New Snowfall to Estimated Meltwater Conversion Table. National Weather Service Observing Handbook Number 7. Surface Observations, Part IV, Table 2-14. U.S. Department of Commerce, 440 pp.

Poulos, G. S., D. A. Wesley, J. S. Snook, and M. P. Meyers, 2002: A Rocky Mountain storm. Part I: The blizzard—Kinematic evolution and the potential for high-resolution numerical forecasting of snowfall. *Wea. Forecasting,* **17,** 955–970.

Reinking, R. F., J. B. Snider, and J. L. Coen, 2000: Influences of storm-embedded orographic gravity waves on cloud liquid water and precipitation. *J. Appl. Meteor.,* **39,** 733–759.

Roebber, P. J., S. L. Bruening, D. M. Schultz, and J. V. Cortinas Jr., 2003: Improving snowfall forecasting by diagnosing snow density. *Wea. Forecasting,* **18,** 264–287.

Rosenfeld, D., and G. Gutman, 1997: Retrieving microphysical properties near the tops of potential rain clouds by multispectral analysis of AVHRR data. *J. Atmos. Sci.,* **34,** 259–283.

Walko, R. L., W. R. Cotton, M. P. Meyers, and J. L. Harrington, 1995: New RAMS cloud microphysics parameterization. Part I: The single-moment scheme. *Atmos. Res.,* **38,** 29–62.

Wetzel, M. A., 1995: Simulation of radiances for future AVHRR platforms with the AVIRIS spectral radiometer. *Int. J. Remote Sens.,* **16,** 1167–1177.

Wood, V. T., R. A. Brown, and S. V. Vasiloff, 2003: Improved detection using negative elevation angles for mountaintop WSR-88Ds. Part II: Simulations of the three radars covering Utah. *Wea. Forecasting,* **18,** 393–403.